

## **CHAPTER 7 - EXPERIMENT 5**

### **CHARACTERIZATION OF THE MICROSTRUCTURE AND MECHANICAL PROPERTIES OF LIQUID PHASE DIFFUSION BONDS USING EUTECTIC Ni-Hf AND Ni-Zr BRAZE ALLOYS AFTER BRAZING FOR 12 HOURS, FOLLOWED BY SOLUTION ANNEALING AND HOT ISOSTATIC PRESSING**

#### **7.1) Introduction**

The results considered in Chapter 6 revealed that a braze microstructure consisting of  $\gamma$  dendrites, surrounded by  $\text{Ni}_5\text{Zr}$  or  $\text{Ni}_7\text{Hf}_2$  intermetallic compound, formed during an extended braze cycle of 12 hours at  $1230^\circ\text{C}$ , followed by solution annealing at the same temperature for 4 hours. These joints displayed promising creep rupture properties, but contained a significant volume fraction of microporosity.

In order to determine whether the properties of the braze joints could be improved by reducing the amount of microporosity, a Hot Isostatic Pressing (HIP) cycle was introduced after solution annealing. During the HIP cycle, the joint was subjected to pressurized argon gas at elevated temperature. The high isostatic gas pressure is known to induce plastic deformation in the material, causing the collapse of any micropores. The success of the HIP cycle was assessed by examining the joint microstructures and by performing elevated temperature tensile and creep rupture tests.

#### **7.2) Experimental procedure**

The liquid phase diffusion bonding technique was used to join In738 parent material using the novel eutectic Ni-Hf and Ni-Zr braze alloys. The In738 plate material and the experimental braze pastes were prepared using the techniques presented in §4.2, and braze samples were produced using the vacuum braze cycle described in §6.2. After joining the brazed samples were placed in a production vacuum furnace equipped with quenching facilities, and solution annealed at  $1230^\circ\text{C}$  for 4 hours, followed by gas quenching at a rate of  $50^\circ\text{C}$  per minute.

The solution heat treatment was followed by a HIP cycle at an isostatic pressure of 104 MPa (15 000 psi), using the following procedure:

- 1) Ramp up to a temperature of  $1080^\circ\text{C}$  at a minimum rate of  $11^\circ\text{C}$  per minute.
- 2) Hold at  $1080^\circ\text{C}$  for 4 hours.
- 3) Quench to room temperature at a rate of  $50^\circ\text{C}$  per minute.

After exposing the plates to the vacuum LPDB, solution heat treatment and HIP cycles described above, samples were sectioned, mounted and polished using conventional metallographic techniques. The polished metallographic samples were then etched with Marble's reagent, and characterized using optical and scanning electron microscopy techniques.

In order to characterize the tensile properties of the braze joints after solution annealing and HIP'ing, tensile tests were performed at room temperature,  $540^\circ\text{C}$ ,  $870^\circ\text{C}$  and  $980^\circ\text{C}$  using the tensile test procedure described in §4.2. Creep rupture tests were performed (as described in

§6.2) using the following combinations of temperature and applied stress: 345 MPa at 845°C; 242 MPa at 900°C; and 138 MPa at 980°C.

### 7.3) Results and discussion

#### 7.3.1 Microstructural investigation:

The microstructure of the Ni-Hf LPDB joint processed at 1230°C for 12 hours, followed by solution annealing and HIP'ing, is shown in **Figures 116 to 119** at various magnifications. The joint consists of MarM247 powder particles, surrounded by layers of Ni-Hf braze alloy. Isolated  $\gamma$  particles are evident within the Ni-Hf braze, but the braze microstructure between the MarM247 powder particles appears to be dominated by  $Ni_7Hf_2$  intermetallic compound.

The microstructure of the LPDB joint produced with MarM247 powder and Ni-Zr braze paste is shown in **Figures 120 to 123** at various magnifications. The original MarM247 powder particles are evident as the lighter, more equiaxed component, while the darker regions consist of eutectic Ni-Zr braze alloy. The braze alloy contains isolated  $\gamma$  dendrites and  $Ni_5Zr$  intermetallic compound.

Isolated micropores were observed in both the Ni-Hf and Ni-Zr joints, suggesting that the HIP cycle was not effective in eliminating microporosity from the braze joints. A higher temperature may be required during the HIP treatment to close the pores formed during the brazing cycle.

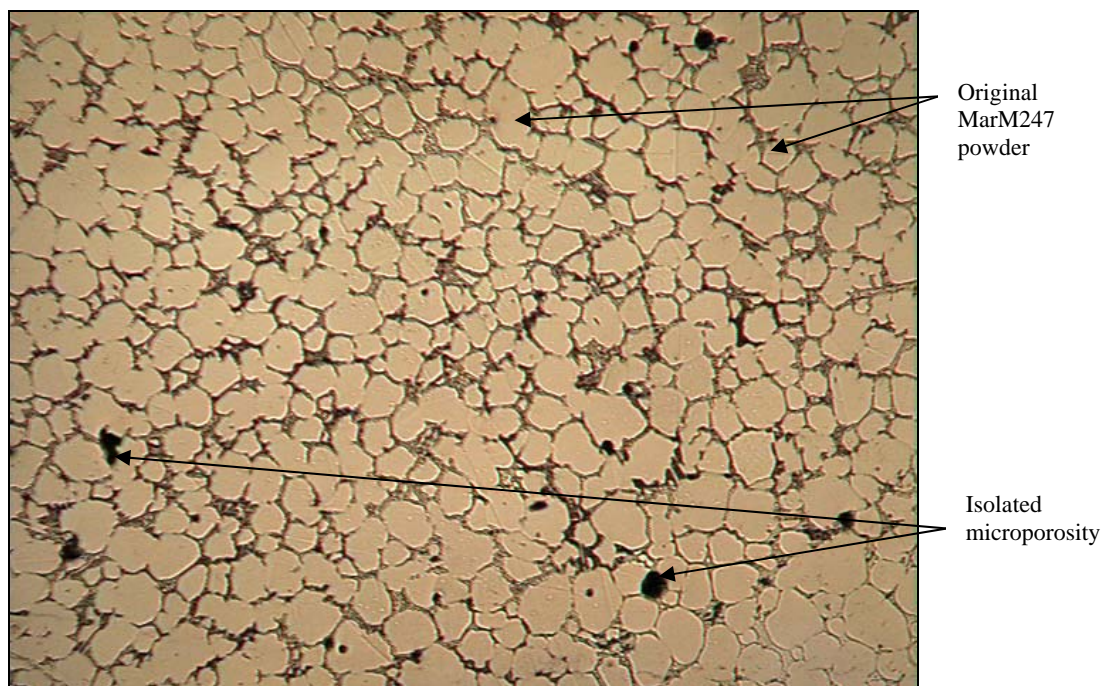


**Figure 116** - Ni-Hf braze dispersed between MarM247 powder particles after brazing at 1230°C for 12 hours, followed by solution heat treatment at 1230°C for 4 hours and a HIP cycle at 1080°C for 4 hours. Magnification: 50X.

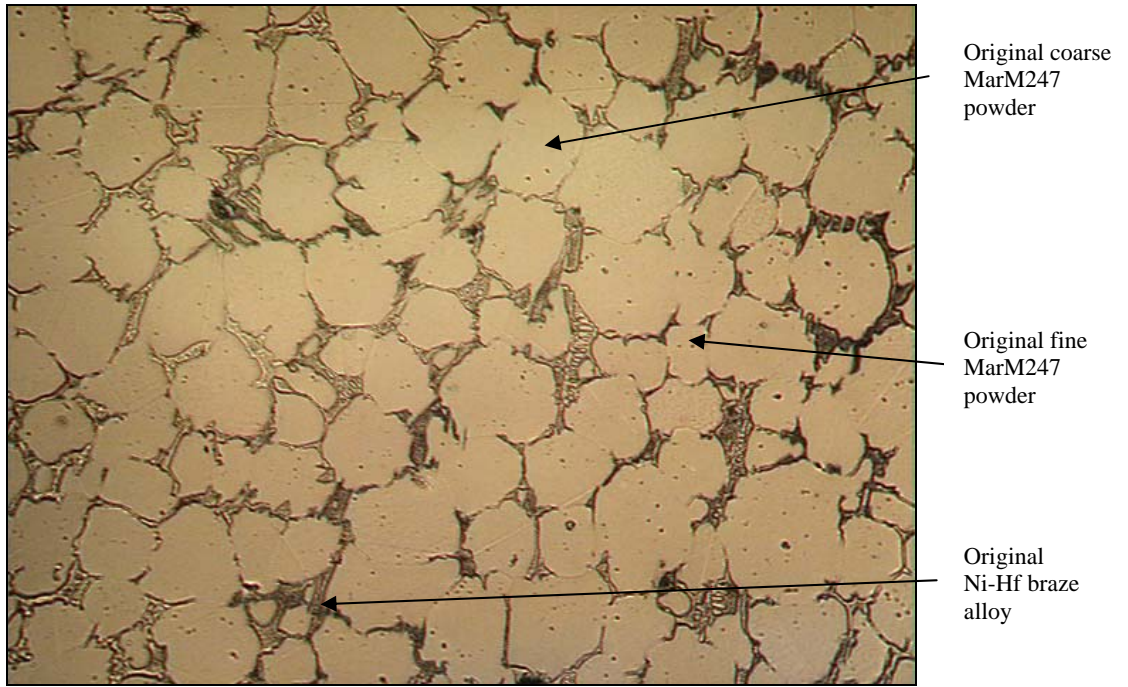


**Figure 117** - Ni-Hf braze dispersed between MarM247 powder particles after brazing at 1230°C for 12 hours, followed by solution heat treatment at 1230°C for 4 hours and a HIP cycle at 1080°C for 4 hours. Magnification: 100X.

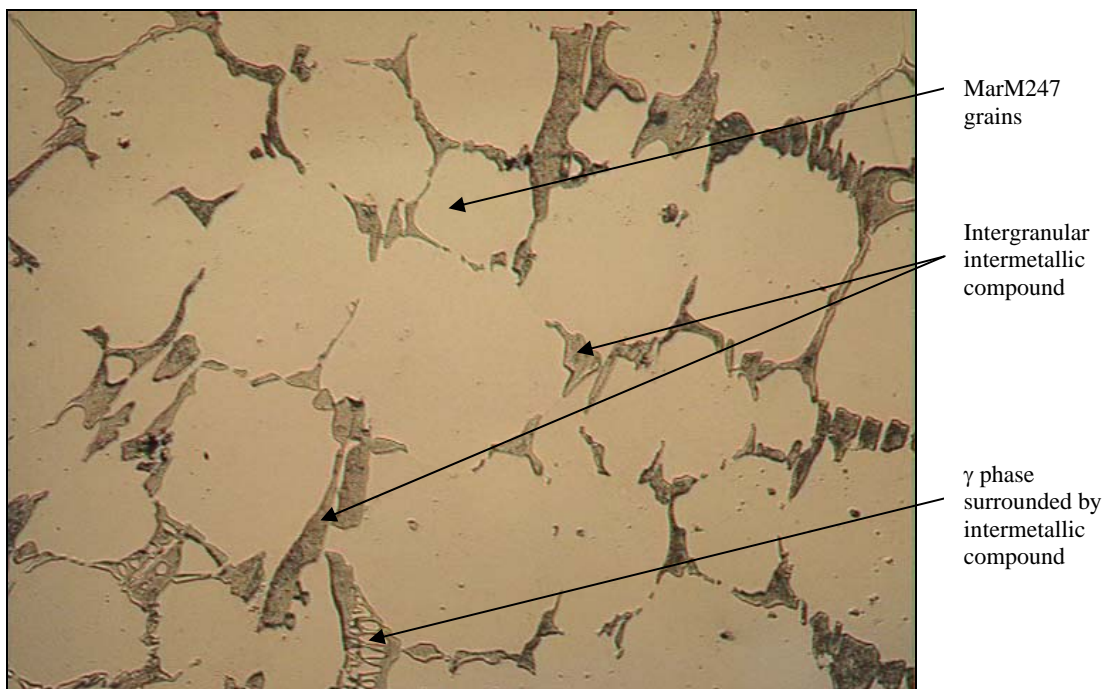


**Figure 118** - Ni-Hf braze dispersed between MarM247 powder particles after brazing at 1230°C for 12 hours, followed by solution heat treatment at 1230°C for 4 hours and a HIP cycle at 1080°C for 4 hours. Magnification: 200X.

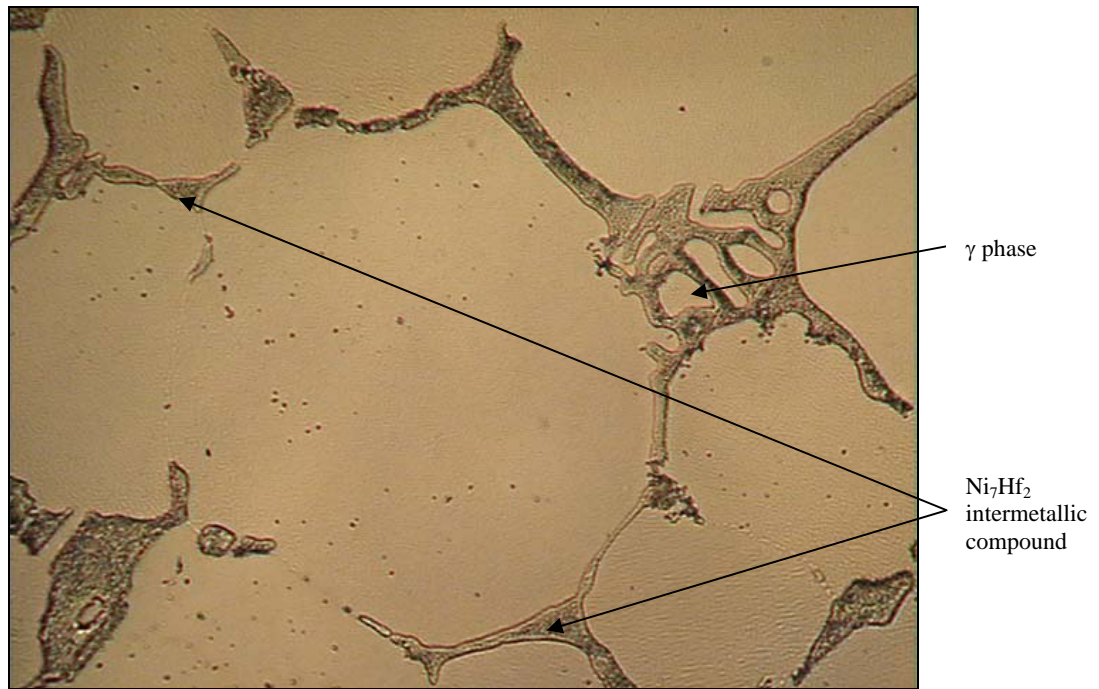


**Figure 119** - Ni-Hf braze dispersed between MarM247 powder particles after brazing at 1230°C for 12 hours, followed by solution heat treatment at 1230°C for 4 hours and a HIP cycle at 1080°C for 4 hours. Magnification: 500X.

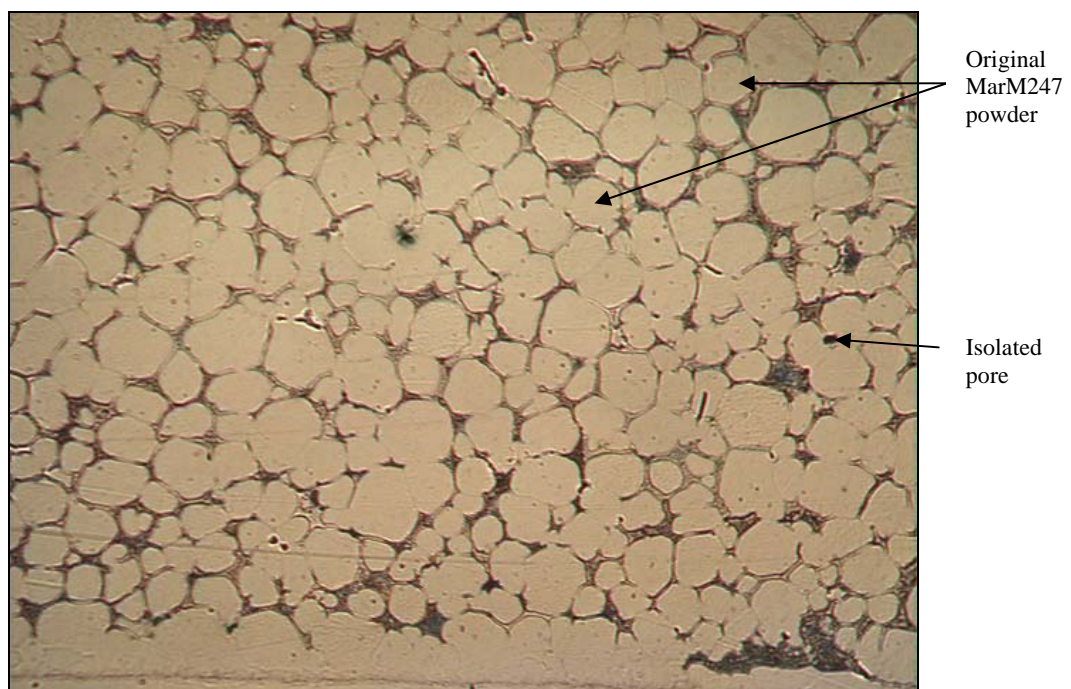


**Figure 120** - Ni-Zr braze dispersed between MarM247 powder particles after brazing at 1230°C for 12 hours, followed by solution heat treatment at 1230°C for 4 hours and a HIP cycle at 1080°C for 4 hours. Magnification: 50X.

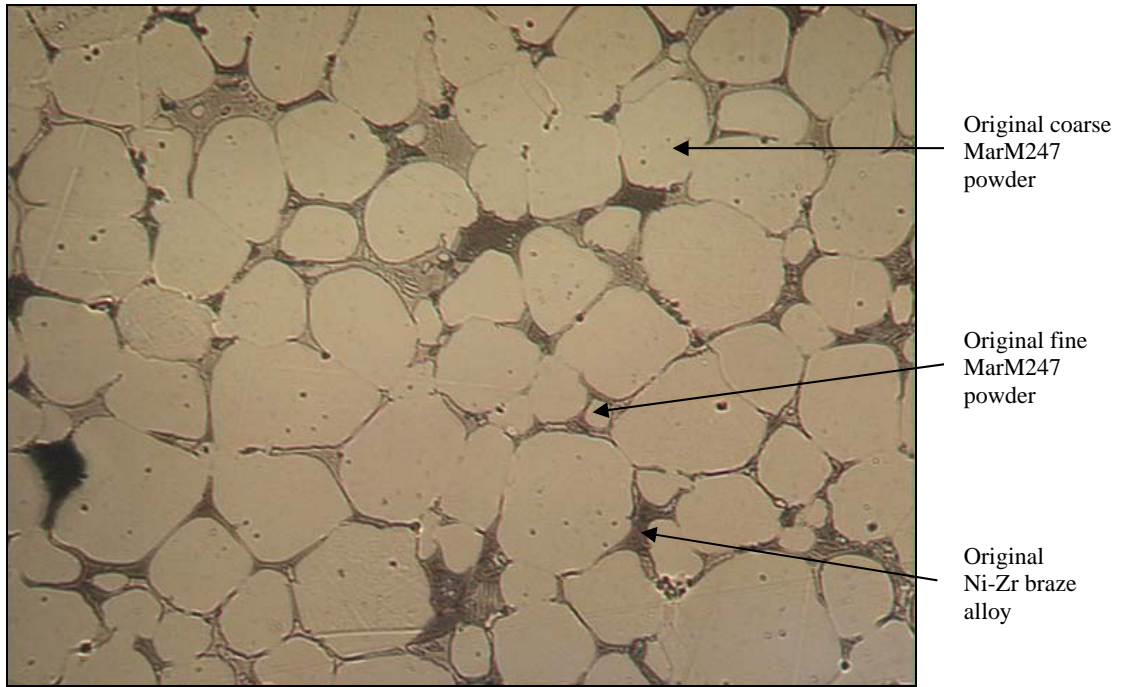


**Figure 121** - Ni-Zr braze dispersed between MarM247 powder particles after brazing at 1230°C for 12 hours, followed by solution heat treatment at 1230°C for 4 hours and a HIP cycle at 1080°C for 4 hours. Magnification: 100X.

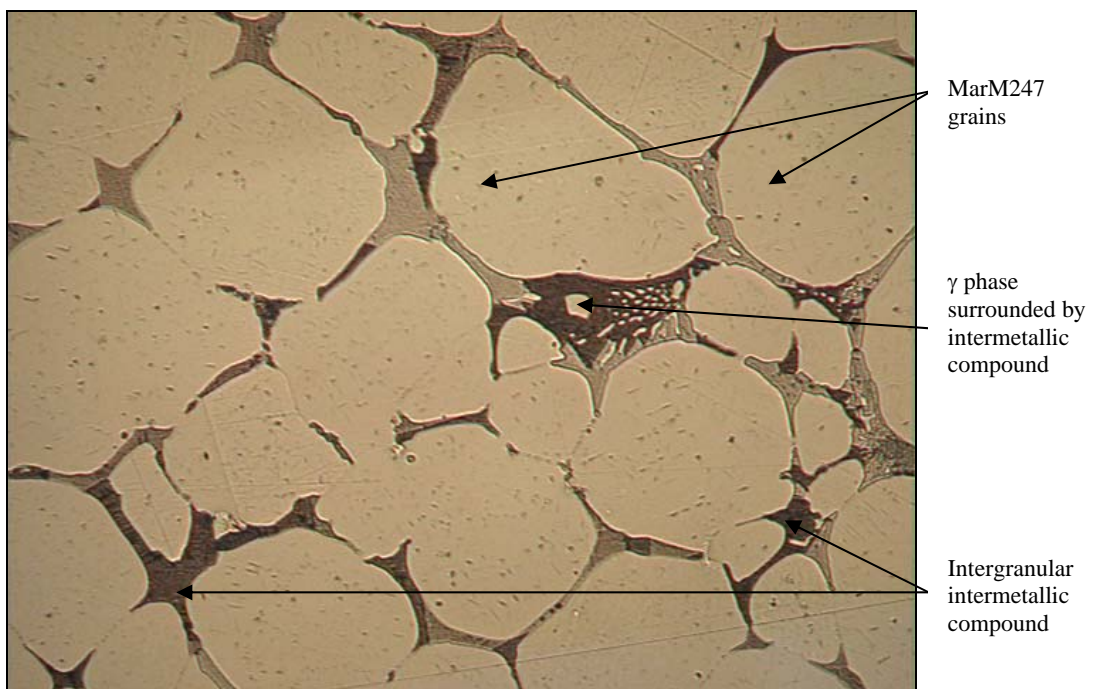


**Figure 122** - Ni-Zr braze dispersed between MarM247 powder particles after brazing at 1230°C for 12 hours, followed by solution heat treatment at 1230°C for 4 hours and a HIP cycle at 1080°C for 4 hours. Magnification: 200X.

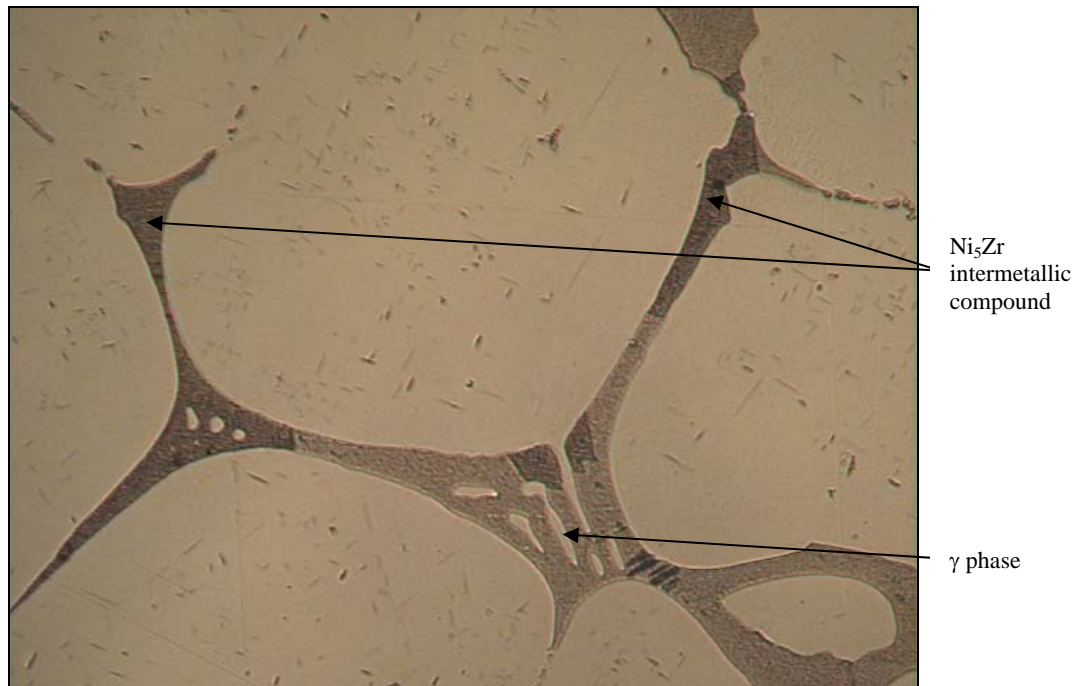


**Figure 123** - Ni-Zr braze dispersed between MarM247 powder particles after brazing at 1230°C for 12 hours, followed by solution heat treatment at 1230°C for 4 hours and a HIP cycle at 1080°C for 4 hours. Magnification: 500X.

SEM micrographs of the Ni-Hf joint, processed at 1230°C for 12 hours, followed by solution heat treatment and HIP'ing, are shown in **Figures 124 and 125**. The intergranular phase highlighted by the arrow in **Figure 124** was shown to have a composition of 52.21Ni-44.72Hf-2.11Co-0.53Cr-0.17Ti-0.26W (wt. %), and was provisionally identified as the Ni<sub>7</sub>Hf<sub>2</sub> intermetallic compound. The micrograph shown in **Figure 125** indicates that a fine, cuboidal gamma prime ( $\gamma'$ ) phase had precipitated within the MarM247  $\gamma$  matrix. The cuboidal and spheroidal  $\gamma'$  precipitates in MarM247 generally form during primary and secondary aging cycles at 1080°C for 4 hours, followed by soaking at 870°C for 24 hours. The HIP cycle used in this investigation therefore overlapped with the primary aging treatment for MarM247, resulting in some  $\gamma'$  precipitation within the  $\gamma$  phase.

**Figure 126** displays a SEM micrograph of the Ni-Zr joint after processing at 1230°C for 12 hours, followed by solution annealing and HIP'ing. The phase identified by the arrow had a composition of 72.18Ni-24.43Zr-2.18Co-0.64Cr-0.45Al-0.28W (wt. %), and was identified as Ni<sub>5</sub>Zr. Although not evident in **Figure 126**, cuboidal  $\gamma'$  precipitates were observed in the MarM247 powder particles at higher magnification.

### 7.3.2 Tensile test results:

The results of tensile tests performed at various temperatures are shown in **Tables 27 to 30**, and presented graphically in **Figures 127 to 130**. The values shown represent the average of three tests at each temperature.

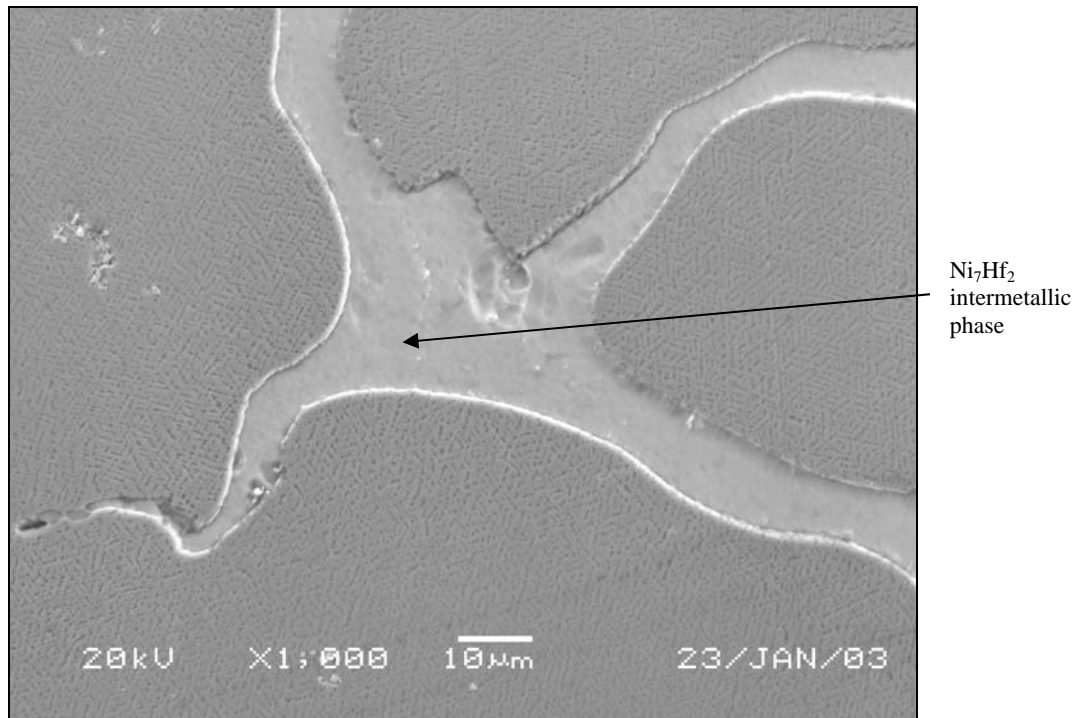


**Figure 124** – SEM micrograph of the Ni-Hf braze, showing the intergranular  $\text{Ni}_7\text{Hf}_2$  intermetallic phase and  $\gamma'$  precipitates within the MarM247 particles.

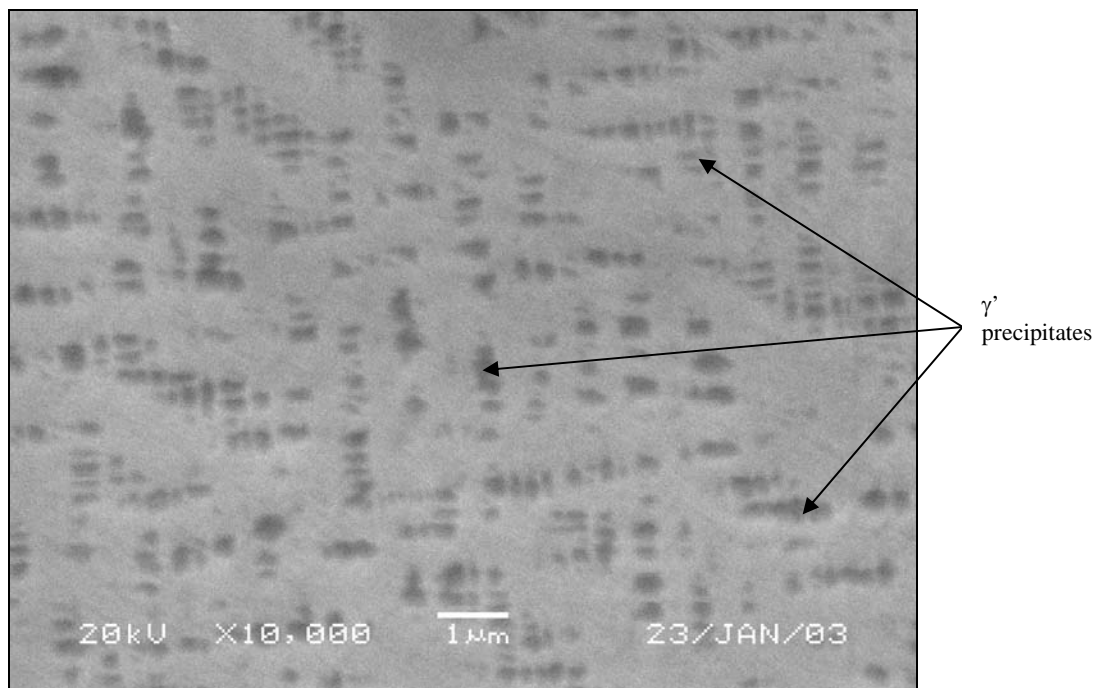


**Figure 125** – Higher magnification SEM micrograph of the Ni-Hf braze, showing cuboidal  $\gamma'$  precipitates within the MarM247 powder particles.

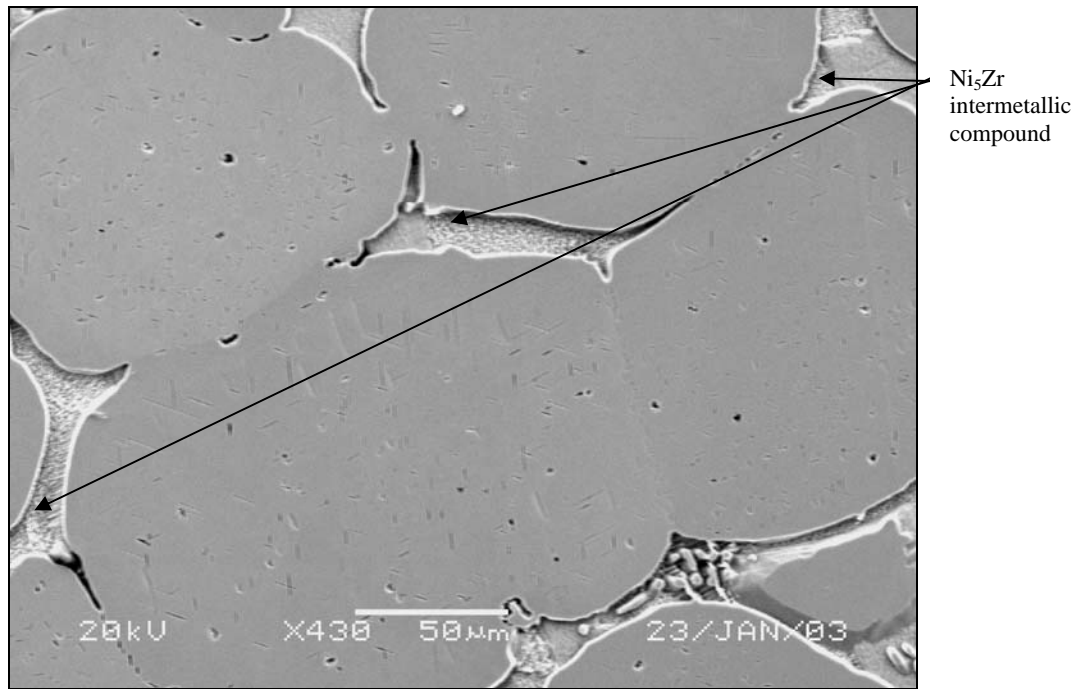


**Figure 126** – SEM micrograph of the Ni-Zr braze, showing intergranular Ni<sub>5</sub>Zr intermetallic compound.

**Table 27** – Joint tensile properties measured at 21°C.

Tensile properties	Ni-Hf joints 1230°C for 40 minutes	Ni-Zr joints 1230°C for 40 minutes	Ni-Hf joints 1230°C for 4 hours	Ni-Zr joints 1230°C for 4 hours	Ni-Hf joints 1230°C for 12 hours + SHT + HIP	Ni-Zr joints 1230°C for 12 hours + SHT + HIP	MarM247 base metal
Tensile strength	323 MPa	557 MPa	344 MPa	564 MPa	713 MPa	736 MPa	960 MPa
Yield strength	239 MPa	505 MPa	302 MPa	511 MPa	644 MPa	622 MPa	800 MPa
Elongation (%)	4.7	3.0	2.7	3.0	2.5	3.7	7.9
Reduction in area (%)	6.3	4.4	3.9	4.5	5.6	8.0	10.0

SHT: Solution heat treatment.

**Table 28** – Joint tensile properties measured at 540°C.

Tensile properties	Ni-Hf joints 1230°C for 40 minutes	Ni-Zr joints 1230°C for 40 minutes	Ni-Hf joints 1230°C for 4 hours	Ni-Zr joints 1230°C for 4 hours	Ni-Hf joints 1230°C for 12 hours + SHT + HIP	Ni-Zr joints 1230°C for 12 hours + SHT + HIP	MarM247 base metal
Tensile strength	328 MPa	619 MPa	406 MPa	625 MPa	740 MPa	999 MPa	1014 MPa
Yield strength	243 MPa	539 MPa	329 MPa	556 MPa	647 MPa	707 MPa	801 MPa
Elongation (%)	3.8	2.7	3.0	2.8	2.7	3.7	7.8
Reduction in area (%)	4.2	3.2	3.8	3.4	5.3	7.9	9.9

SHT: Solution heat treatment.



**Table 29** – Joint tensile properties measured at 870°C.

Tensile properties	Ni-Hf joints 1230°C for 40 minutes	Ni-Zr joints 1230°C for 40 minutes	Ni-Hf joints 1230°C for 4 hours	Ni-Zr joints 1230°C for 4 hours	Ni-Hf joints 1230°C for 12 hours + SHT + HIP	Ni-Zr joints 1230°C for 12 hours + SHT + HIP	MarM247 base metal
Tensile strength	289 MPa	444 MPa	342 MPa	480 MPa	544 MPa	743 MPa	790 MPa
Yield strength	211 MPa	414 MPa	277 MPa	404 MPa	458 MPa	650 MPa	650 MPa
Elongation (%)	2.0	1.0	2.2	2.1	2.4	3.4	5.0
Reduction in area (%)	3.0	2.4	3.2	3.1	4.2	6.0	7.7

SHT: Solution heat treatment.

**Table 30** – Joint tensile properties measured at 980°C.

Tensile properties	Ni-Hf joints 1230°C for 40 minutes	Ni-Zr joints 1230°C for 40 minutes	Ni-Hf joints 1230°C for 4 hours	Ni-Zr joints 1230°C for 4 hours	Ni-Hf joints 1230°C for 12 hours + SHT + HIP	Ni-Zr joints 1230°C for 12 hours + SHT + HIP	MarM247 base metal
Tensile strength	195 MPa	261 MPa	266 MPa	308 MPa	282 MPa	311 MPa	506 MPa
Yield strength	141 MPa	245 MPa	206 MPa	214 MPa	223 MPa	239 MPa	312 MPa
Elongation (%)	1.8	0.8	2.7	3.1	4.3	4.8	4.7
Reduction in area (%)	2.9	1.9	3.1	6.2	5.7	2.9	7.5

SHT: Solution heat treatment.

The tensile strength and yield stress of the MarM247 base metal, and the MarM247/Ni-Hf and MarM247/Ni-Zr joints in various conditions, are shown in **Figures 127 and 128** as a function of test temperature. It is evident that the HIP cycle improved the tensile and yield strengths of both joints at all test temperatures, with the strength values approaching those of the base metal at elevated temperatures. The MarM247/Ni-Zr joints displayed higher tensile and yield strengths than the Ni-Hf joints at almost all test temperatures. With an increase in test temperature, the tensile strength of the MarM247/Ni-Zr joints after the HIP cycle varied from 98% of the base metal tensile strength at 540°C, to 94% at 870°C, and 62% at 980°C. Measured yield strength values ranged from 88% of the base metal yield stress at 540°C, to 100% at 870°C, and 77% at 980°C for the Ni-Zr joints following the HIP cycle. Corresponding strength measurements for the MarM247/Ni-Hf joints ranged from 73% and 81% of the base metal properties (for tensile strength and yield stress, respectively) at 540°C, to 69% and 71% at 870°C, and 56% and 72% at 980°C. The increase in strength after the HIP cycle can most likely be attributed to precipitation hardening linked to the formation of fine  $\gamma'$  precipitates in the MarM247 powder particles during the HIP treatment.

As shown in **Figures 129 and 130**, the HIP cycle generally resulted in an improvement in the ductility of the braze joints, particularly at elevated temperatures. The MarM247/Ni-Hf braze joints displayed approximately 45% of the ductility of the base metal at 540°C, increasing to 51% at 870°C, and finally to 84% at 980°C. The ductility of the MarM247/Ni-Zr joints ranged from approximately 64% of the base metal ductility at 540°C, to 73% at 870°C, and almost 100% at 980°C (calculation based on the percentage elongation). The increase in ductility measured at elevated test temperatures is probably associated with the observed decrease in strength.

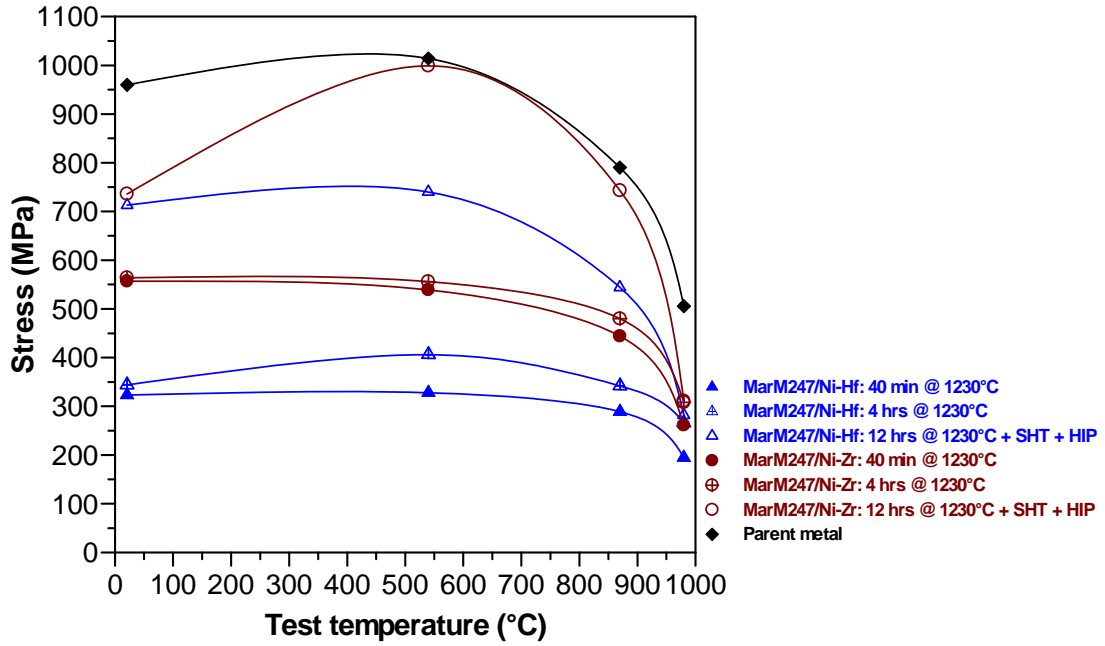


**Figure 127** – The tensile strength of the MarM247 base metal, and the MarM247/Ni-Hf and MarM247/Ni-Zr braze joints after brazing for 40 minutes and 4 hours at 1230°C, and after brazing for 12 hours at 1230°C, followed by solution heat treatment and a HIP cycle.

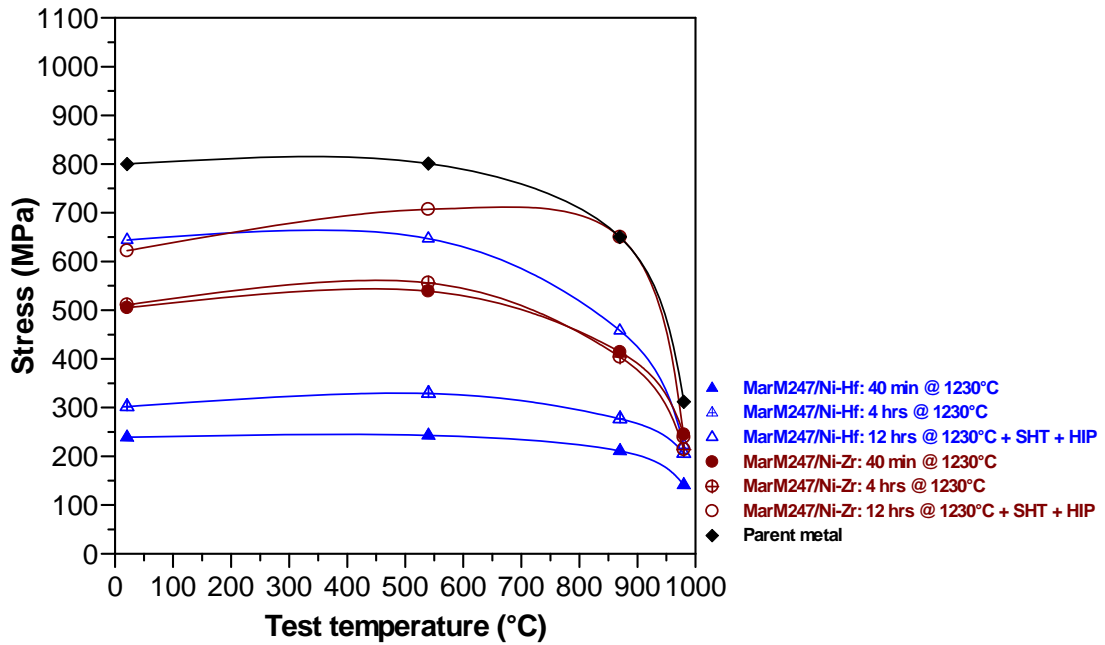


**Figure 128** – The yield stress of the MarM247 base metal, and the MarM247/Ni-Hf and MarM247/Ni-Zr braze joints after brazing for 40 minutes and 4 hours at 1230°C, and after brazing for 12 hours at 1230°C, followed by solution heat treatment and a HIP cycle.

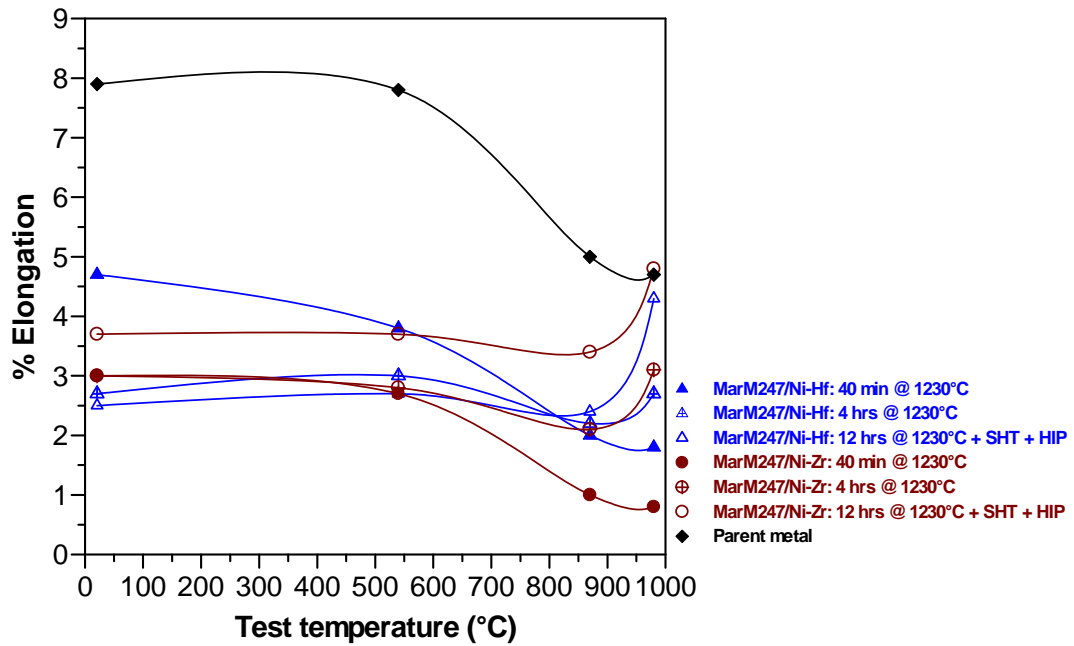


**Figure 129** – The percentage elongation of the MarM247 base metal, and the MarM247/Ni-Hf and MarM247/Ni-Zr braze joints after brazing for 40 minutes and 4 hours at 1230°C, and after brazing for 12 hours at 1230°C, followed by solution heat treatment and a HIP cycle.

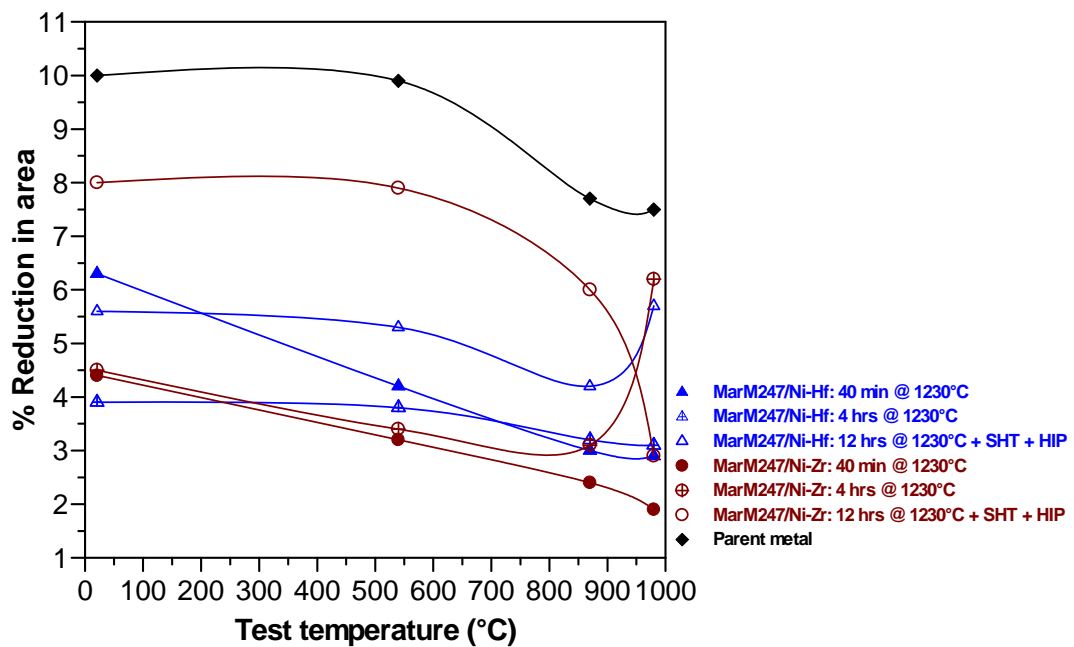


**Figure 130** – The percentage reduction in area of the MarM247 base metal, and the MarM247/Ni-Hf and MarM247/Ni-Zr braze joints after brazing for 40 minutes and 4 hours at 1230°C, and after brazing for 12 hours at 1230°C, followed by solution heat treatment and a HIP cycle.

### 7.3.3 Creep rupture test properties:

The results of creep rupture tests performed at various temperatures and applied stress levels are shown in **Table 31** and presented graphically in the form of a Larson-Miller plot in **Figure 131**.

**Table 31** – The influence of a HIP cycle on the creep rupture properties of the In738 base metal and the MarM247/Ni-Hf and MarM247/Ni-Zr joints (1.5 mm joint gap).

Test condition	Property	Ni-Hf 1230°C for 12 hours + SHT	Ni-Hf 1230°C for 12 hours + SHT + HIP	Ni-Zr 1230°C for 12 hours + SHT	Ni-Zr 1230°C for 12 hours + SHT + HIP	In738 base metal
345 MPa at 845°C	Creep rupture life	18.6 hours	20.2 hours	21.2 hours	24.4 hours	27.4 hours
	% Elongation	3.7	3.8	3.4	3.9	5.5
	% Reduction in area	5.6	5.6	4.4	4.7	7.3
242 MPa at 900°C	Creep rupture life	19.0 hours	19.4 hours	20.5 hours	22.1 hours	29.8 hours
	% Elongation	4.6	4.3	4.1	4.2	5.7
	% Reduction in area	6.1	5.8	5.3	6.7	7.9
138 MPa at 980°C	Creep rupture life	13.6 hours	14.8 hours	16.5 hours	17.7 hours	21.2 hours
	% Elongation	6.6	7.0	5.1	8.0	8.1
	% Reduction in area	9.3	24.7	7.1	23.5	11.8

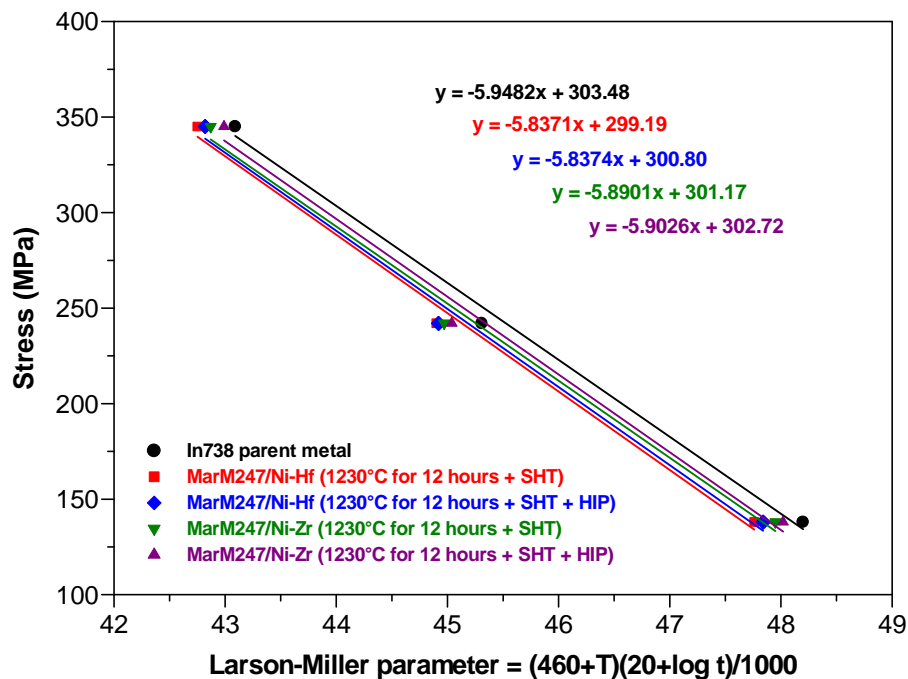


**Figure 131** – Larson-Miller plot for the In738 base metal and the MarM247/Ni-Hf and MarM247/Ni-Zr joints after brazing for 12 hours at 1230°C, followed by solution heat treatment (SHT) and a HIP cycle.

The results shown in **Table 31** and in **Figure 131** illustrate that the HIP cycle resulted in an improvement in the creep rupture properties of both the Ni-Hf and Ni-Zr braze joints. The best creep rupture properties were obtained in the MarM247/Ni-Zr joints after brazing at 1230°C for 12 hours, followed by a solution heat treatment at 1230°C for 4 hours and a HIP

cycle at 1080°C for 4 hours. Depending on the test temperature, these joints displayed creep rupture lives between 74% and 89% of that of the base metal. Since the joints were tested in the partially age hardened condition, the creep rupture properties are expected to improve further once the full aging heat treatment is employed.

Although linear regression methods revealed very little statistically relevant difference between the lines representing the braze joints in **Figure 131**, the Larson-Miller plot can be used to rank the braze joints in order of descending creep rupture properties:

- MarM247/Ni-Zr joint brazed at 1230°C for 12 hours, followed by solution heat treatment and a HIP cycle.
- MarM247/Ni-Zr joint brazed at 1230°C for 12 hours, followed by solution heat treatment.
- MarM247/Ni-Hf joint brazed at 1230°C for 12 hours, followed by solution heat treatment and a HIP cycle.
- MarM247/Ni-Hf joint brazed at 1230°C for 12 hours, followed by solution heat treatment.

It is important to note that the improved creep rupture properties displayed by the braze joints after the HIP cycle cannot be attributed to the closure of micropores in the microstructure. The higher creep rupture properties are most likely due to the precipitation of fine  $\gamma'$  precipitates within the MarM247 powder particles during the HIP cycle.

Although equivalent base metal creep properties were not achieved, excellent joint ductility was obtained. For example, during testing at an applied stress level of 138 MPa at 980°C, both the Ni-Zr and Ni-Hf braze joints displayed ductility values in the region of 87% of that of the base metal. This implies that the presence of the  $\text{Ni}_7\text{Hf}_2$  or  $\text{Ni}_5\text{Zr}$  intermetallic compound within the braze alloy did not embrittle the joints to the same extent as the boride phases observed in Ni-B braze alloys. In boride-containing braze joints, the ductility values rarely exceed 30% of the ductility of the base metal in the case of wide joint gaps.

#### 7.4) Conclusions

- Brazing for 12 hours at 1230°C, followed by solution heat treatment at 1230°C for 4 hours and a HIP cycle at 1080°C for 4 hours, resulted in joint microstructures consisting of MarM247 powder particles, surrounded by eutectic Ni-Hf or Ni-Zr braze alloy containing  $\gamma$  phase and  $\text{Ni}_7\text{Hf}_2$  or  $\text{Ni}_5\text{Zr}$  intermetallic compound. The extended braze cycle and the solution annealing treatment reduced the fraction of  $\gamma$  phase and the amount of intermetallic compound between the MarM247 particles, resulting in a less continuous film of braze alloy surrounding the MarM247 grains. The HIP cycle induced the precipitation of fine  $\gamma'$  precipitates within the MarM247 powder particles.
- The HIP cycle was not effective in eliminating microporosity from the joint. The HIP temperature may have been too low to close the micropores formed during brazing.
- The HIP cycle significantly improved the tensile and yield strength values of both joints at all test temperatures, with the strength values approaching those of the base metal at elevated temperatures. The MarM247/Ni-Zr joints displayed higher tensile and yield strengths than the Ni-Hf joints at almost all test temperatures. The increase in strength

after the HIP cycle can most likely be attributed to precipitation hardening linked to the formation of fine  $\gamma'$  precipitates in the MarM247 powder particles during the HIP treatment. The HIP cycle generally resulted in an improvement in the ductility of the braze joints, particularly at elevated temperatures. The increase in ductility measured at elevated test temperatures is probably associated with the observed decrease in strength.

- The HIP treatment resulted in an improvement in the creep rupture properties of both the Ni-Hf and Ni-Zr braze joints. The best creep rupture properties were obtained in the MarM247/Ni-Zr joints. Depending on the test temperature, these joints displayed creep rupture properties between 74% and 89% of those of the base metal. Since the joints were tested in the partially age hardened condition, the creep rupture properties are expected to improve further once the full aging heat treatment is employed. Although equivalent base metal creep properties were not achieved, excellent joint ductility was obtained, suggesting that the presence of the  $\text{Ni}_7\text{Hf}_2$  or  $\text{Ni}_5\text{Zr}$  intermetallic compound within the braze alloy does not embrittle the joints to the same extent as the boride phases observed in Ni-B braze alloys.
- The majority of cracks which form in turbine components during service initiate under low cycle fatigue conditions. The low cycle fatigue properties of braze repaired turbine components therefore ultimately determine whether a braze alloy can be commercialized successfully. Experiment 6, described in Chapter 8, aimed at determining the low cycle fatigue (LCF) properties of the novel braze alloys. In order to obtain representative LCF results, the thermal treatment of the braze joints was optimized based on the results of earlier experiments. The braze time was increased to 24 hours (to promote diffusion of the melt point depressants into the parent metal), the HIP temperature was raised to 1200°C (to eliminate microporosity) and the joints were subjected to the complete primary and secondary aging cycles to precipitate  $\gamma'$  in the MarM247 powder particles.

## **CHAPTER 8 - EXPERIMENT 6**

### **CHARACTERIZATION OF THE LOW CYCLE FATIGUE PROPERTIES OF LIQUID PHASE DIFFUSION BONDS USING EUTECTIC Ni-Hf AND Ni-Zr BRAZE ALLOYS AFTER BRAZING FOR 24 HOURS, FOLLOWED BY SOLUTION ANNEALING, HOT ISOSTATIC PRESSING AT 1200°C AND A FULL AGING TREATMENT**

#### **8.1) Introduction**

The results of Experiment 5, described in Chapter 7, revealed that brazing at 1230°C for 12 hours, followed by solution annealing at 1230°C for 4 hours and a HIP treatment at 1080°C for 4 hours, resulted in a microstructure consisting of MarM247 powder particles, interspersed with Ni-Hf or Ni-Zr braze alloy. The layers of braze alloy surrounding the MarM247 powder particles appeared less continuous than those observed during Experiment 4, containing a lower volume fraction of  $\gamma$  phase and Ni<sub>5</sub>Zr or Ni<sub>7</sub>Hf<sub>2</sub> intermetallic compound. The HIP cycle used in Experiment 5 overlapped with the primary aging cycle for MarM247, resulting in the precipitation of fine  $\gamma'$  particles within the MarM247 grains. The braze joints displayed promising tensile and creep rupture properties, despite being only partially age hardened.

The aim of Experiment 6 was to determine the low cycle fatigue (LCF) properties of the braze joints. Low cycle fatigue testing is essential since cracks in nozzle segments almost always initiate under LCF conditions, and nozzle segments rarely fail under tensile overload or creep rupture conditions. Tensile and creep rupture tests provide the approval authority with an indication of the potential of novel braze alloys, but ultimately it is the low cycle fatigue test results which determine whether a braze alloy will be commercialized. In order to obtain representative LCF results, the thermal treatment of the braze joints was optimized based on the results of earlier experiments. The braze cycle was extended to 24 hours at 1230°C to facilitate diffusion of the melt point depressant (Hf or Zr) into the parent metal, followed by solution annealing at the same temperature for 4 hours. The braze joints were then subjected to a 4 hour HIP treatment. Since the HIP cycle used in Experiment 5 was not effective in eliminating microporosity, the HIP temperature was increased to 1200°C. After the HIP treatment, the specimens were subjected to the full MarM247 aging treatment designed to precipitate a mixture of coarse and fine  $\gamma'$  particles.

#### **8.2) Experimental procedure**

During the course of this investigation, In738 plates with dimensions of approximately 240 mm long, 125 mm wide and 15 mm thick were prepared. A 1.5 mm wide groove was machined along the length of the plate, as shown in **Figures 132 and 133**. After machining, the groove was grit blasted with 220 grit silicon carbide media, and wiped with acetone to remove any grit blasting residue.

MarM247 paste was prepared from a mixture of coarse and fine MarM247 powder (as described in §4.2) and used to fill the groove machined in each In738 plate. After drying, a layer of eutectic Ni-Hf braze alloy, Ni-Zr braze alloy or commercially available BRB braze alloy in paste form was applied over the MarM247 powder. As described in Chapter 1, BRB is a B-containing braze of nominal composition Ni-13.5Cr-7.5Co-4Al-2.5B. The plates were dried, and subjected to the following vacuum braze cycle:

1. Ramp up to a temperature of 450°C at a minimum rate of 9°C/minute.
2. Hold at 450°C for 20 minutes to allow the binder to burn off.
3. Ramp up to a temperature of 1150°C at a minimum rate of 9°C/minute.
4. Hold at 1150°C for 20 minutes to allow the samples to stabilize at this temperature.
5. Ramp up to a temperature of 1230°C at a minimum rate of 9°C/minute to melt the Ni-Hf and Ni-Zr braze alloys and to allow the melt to infiltrate the MarM247 powder.
6. Hold at 1230°C for 24 hours.
7. Furnace cool to room temperature.



**Figure 132** – In738 plate with a 1.5 mm wide groove machined in the center.



**Figure 133** – Enlarged view of the 1.5 mm wide groove machined in the centre of the In738 plate samples.

The brazed plates were transferred to a production furnace and solution annealed at 1230°C for 4 hours, followed by gas quenching. The solution annealed samples were then subjected to a revised HIP cycle at a pressure of 104 MPa (15000 psi), as described below:

1. Ramp up to a temperature of 1200°C at a minimum rate of 11°C/minute.
2. Hold at 1200°C for 4 hours.
3. Gas quench as rapidly as possible using argon gas at 2 bar pressure.

Following the HIP cycle, the plates were subjected to the primary and secondary aging heat treatments used in industry to precipitate a combination of fine and coarse  $\gamma'$  precipitates in MarM247. The primary aging heat treatment involves holding the material at 1080°C for 4 hours, followed by gas quenching. This aging cycle is followed by the secondary aging heat



treatment, during which the samples are held at 870°C for 20 hours, followed by gas quenching.

After thermal processing, 12.7 mm diameter low cycle fatigue test specimens were machined from the plates in such a way that each braze joint formed a full butt joint in the centre of the gauge length. The ends of the samples were threaded and the diameter of the gauge length reduced to 6.35 mm (as shown in **Figure 134**).

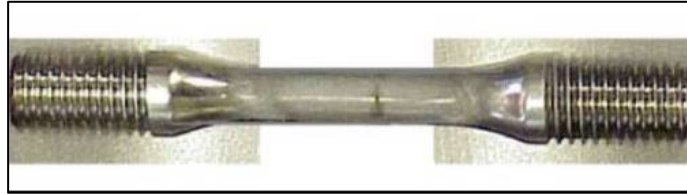


**Figure 134** - LCF specimen with the braze joint in the centre of the gauge length.

Low cycle fatigue tests were performed at a test temperature of 870°C under strain control conditions. The tests were performed at a constant strain rate of 0.01 s<sup>-1</sup> with a symmetrical triangular waveform. The total strain was varied from 0.3% to 2% and the test frequency from 1 Hz to 0.33 Hz. A constant A-ratio (defined below) of +1 was maintained during testing.

$$\text{A-ratio} = (\text{maximum strain} - \text{minimum strain}) / (\text{maximum strain} + \text{minimum strain})$$

### 8.3) LCF test results:

The results of the LCF tests for the In738 base metal, and the MarM247/Ni-Hf, MarM247/Ni-Zr and In738/BRB braze joints, are displayed graphically in **Figure 135**.

The In738 base metal displayed the best LCF properties, whereas the In738/BRB braze joint had the lowest LCF properties. BRB is a B-containing braze filler metal with a known tendency to form brittle borides in wide gap brazed joints. These boride phases are hard and brittle, and have a detrimental effect on the LCF properties. The Ni-Hf braze joint displayed slightly higher LCF life than the Ni-Zr braze joint.

The LCF graph shown in **Figure 135** can be divided into three regions:

- Below a strain of 0.4%, the BRB braze joint exhibited 70% of the fatigue life of the base metal, compared to 85% for the MarM247/Ni-Zr braze, and 96% for the MarM247/Ni-Hf braze joint. Different repair authorities normally have different acceptance and rejection criteria, but it is safe to say that if a braze joint displays 70% or more of the base metal's LCF life, the braze filler can be utilized for production braze repairs of cracks in stationary nozzle segments. Unfortunately, only a small number of cracks are normally located in regions of nozzles where the strain is less than 0.4%.
- Between 0.4% and 0.8% strain, the BRB braze joint exhibited only 11% of the base metal's life, whereas the MarM247/Ni-Zr braze displayed 70% and the MarM247/Ni-Hf braze 74% of the base metal's low cycle fatigue life. The majority of cracks in nozzle

segments occur in this strain range, suggesting that both the Ni-Zr and Ni-Hf braze filler metals are likely to outperform the B-containing braze alloy in service.

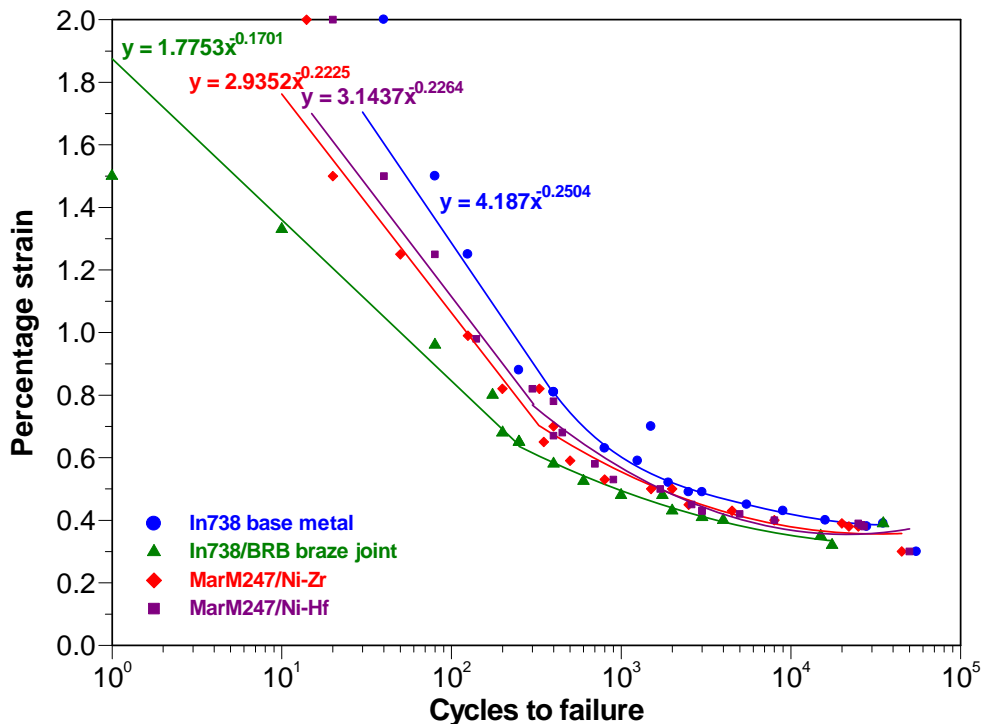


**Figure 135** – Low cycle fatigue properties of the In738 base metal, the In738/BRB braze joint, and the MarM247/Ni-Zr and MarM247/Ni-Hf braze joints.

- Between 0.8% and 2% strain, representing the region of a nozzle segment where one or two cracks typically form during service, none of the braze joints evaluated displayed good LCF life. At a strain level of 1.5%, the BRB braze joint failed after only 1 cycle, whereas the Ni-Zr and Ni-Hf braze joints failed after 30 and 40 cycles, respectively. The base metal failed after 80 cycles at this strain level, indicating that none of the three braze filler metals evaluated approach the LCF properties of the base metal at high strains. Nevertheless, the Ni-Zr and Ni-Hf braze joints outperformed the BRB braze joint by an order of magnitude, suggesting improved performance and easier acceptance compared to the commercially available B-containing BRB braze filler metal.

#### 8.4) Conclusions

- Since cracks in nozzle segments generally initiate under low cycle fatigue conditions, a braze joint should ideally display LCF properties equivalent or better than those of the base metal. Since the original cracks in a nozzle segment form in the base metal, a repaired area with inferior LCF properties compared to those of the base metal will result in earlier crack initiation and faster crack propagation.
- The measured LCF properties of the B-containing BRB braze were vastly inferior to those of the base metal, with the In738/BRB braze joint displaying a low cycle fatigue life of only 1 cycle at an applied strain of 1.5%, compared to 80 cycles for the base metal at the same level of strain. Although the Ni-Zr and Ni-Hf braze joints displayed superior LCF properties at high strains compared to the BRB joints, the LCF properties of the

novel braze alloys at high strains were only 27% and 50%, respectively, of the base metal's LCF properties.

- At intermediate strain levels (0.4% to 0.8% strain), the Ni-Zr and Ni-Hf braze joints displayed 70% and 74%, respectively, of the LCF properties of the base metal. At these strain levels, the novel alloys outperformed the BRB braze alloy that displayed only 11% of the base metal's LCF properties.
- At low strain rates (0.2% to 0.4% strain), the Ni-Zr and Ni-Hf braze joints displayed LCF properties equivalent to those of the base metal, whereas the BRB joint exhibited approximately 70% of the base metal's LCF properties.
- Although the Ni-Zr or Ni-Hf braze alloys did not display LCF properties equivalent to those of the base metal at high strain values, the novel braze filler metals outperformed the commercially available B-containing BRB braze alloy. The new alloys should therefore have a distinct advantage over the B-containing braze filler metals in the repair of nozzle segments in industry.
- The good ductility values and promising LCF properties of LPDB joints produced using the novel braze alloys suggested that it may be possible to further improve the joint ductility by combining the braze paste with a ductile solid solution strengthened Ni-base superalloy within the joint, rather than the  $\gamma'$ -strengthened MarM247 powder evaluated in previous chapters. The results of such a change in joint matrix alloy are presented in Chapter 9.

## CHAPTER 9 - EXPERIMENT 7

### **CHARACTERIZATION OF THE MECHANICAL PROPERTIES OF LIQUID PHASE DIFFUSION BONDS PRODUCED BY MIXING A SOLID SOLUTION STRENGTHENED NICKEL-BASE SUPERALLOY POWDER WITH THE EUTECTIC Ni-Hf AND Ni-Zr BRAZE ALLOYS**

#### **9.1) Introduction**

During the preceding experiments, described in Chapters 4 to 8, a precipitation hardenable,  $\gamma'$ -strengthened Ni-base superalloy powder, known as MarM247, was mixed with the eutectic Ni-Zr or Ni-Hf braze alloy within the joint in an attempt to produce high-strength braze joints with good ductility. As a possible alternative, a ductile solid solution strengthened superalloy powder, such as Haynes 230, may be substituted for the MarM247 powder in an attempt to improve the ductility of the joint.

Experiment 9 therefore aimed to compare the mechanical properties (and in particular the ductility) of MarM247/Ni-Zr joints with Haynes 230/Ni-Zr joints in order to determine whether a braze joint with a solid solution strengthened matrix (in lieu of a  $\gamma'$ -strengthened matrix) displays a higher level of ductility.

#### **9.2) Experimental procedure**

In738 plate material was produced and prepared as described in §3.2. A mixture of coarse and fine Haynes 230 Ni-base superalloy powder with a nominal composition shown in **Table 32** was mixed with braze binder to form a paste. The Haynes 230 paste was applied to the In738 plate over an area of approximately 2500 mm<sup>2</sup> and allowed to dry. A layer of eutectic Ni-Zr braze alloy in paste form (produced as described in §3.2) was then applied over the dry Haynes 230 powder. The samples were dried for one hour, and placed in a laboratory vacuum furnace.

**Table 32** – Nominal chemical composition of the Haynes 230 powder used in this investigation (wt.%, balance Ni).

<b>B</b>	<b>C</b>	<b>Co</b>	<b>Cr</b>	<b>Mn</b>	<b>Mo</b>	<b>Al</b>	<b>W</b>	<b>La</b>	<b>Si</b>	<b>Fe</b>
0.015	0.1	5.0	22.0	0.5	2.0	0.3	14.0	0.02	0.4	3.0

The vacuum braze cycle used was as follows:

- 1) Ramp up to a temperature of 450°C at a minimum rate of 9°C/minute.
- 2) Hold at 450°C for 20 minutes to allow the binder to burn off.
- 3) Ramp up to a temperature of 1150°C at a minimum rate of 9°C/minute.
- 4) Hold at 1150°C for 20 minutes to allow the samples to stabilize at this temperature.
- 5) Ramp up to a temperature of 1230°C at a minimum rate of 9°C/minute to melt the Ni-Zr braze alloy and to allow the melt to infiltrate the Haynes 230 powder particles.
- 6) Hold at 1230°C for 12 hours.
- 7) Furnace cool to room temperature.

After brazing, the samples were transferred to a production vacuum furnace equipped with quenching facilities in order to solution anneal the joint. Gas quenching, using 2 bar argon pressure, was utilized on completion of the solution annealing cycle. The solution heat treatment used in this experiment was as follows:

- 1) Ramp up to a temperature of 1230°C at a minimum rate of 14°C per minute.
- 2) Hold at 1230°C for 4 hours.
- 3) Quench to room temperature at a minimum rate of 50°C per minute.

The solution heat treatment was followed by a HIP cycle at an isostatic pressure of 104 MPa (15 000 psi), using the following procedure:

- 1) Ramp up to a temperature of 1080°C at a minimum rate of 11°C per minute.
- 2) Hold at 1080°C for 4 hours.
- 3) Quench to room temperature at a rate of 50°C per minute.

In order to characterize the tensile properties of the braze joint after solution annealing and HIP'ing, tensile tests were performed at room temperature, 95°C, 315°C, 540°C, 650°C, 870°C and 980°C using the tensile test procedure described in §4.2. Creep rupture tests were performed (as described in §6.2) using the combinations of test temperature and applied stress shown in **Table 33**. These temperature/stress combinations were selected because the creep rupture properties of the standard Haynes 230 alloy under these test conditions have been documented.

**Table 33** – Creep rupture test conditions.

Test temperature	Applied stress
650°C	385 MPa (56 ksi)
760°C	185 MPa (27 ksi)
870°C	95 MPa (14 ksi)
980°C	41 MPa (6.0 ksi)
1040°C	24 MPa (3.5 ksi)
1095°C	14 MPa (2.1 ksi)

### 9.3) Results and discussion

#### 9.3.1 Tensile test results:

The results of tensile tests performed at various temperatures are shown in **Tables 34 to 40**, and are presented graphically in **Figures 136 to 138**. The values shown represent the average of three tests at each temperature.

**Table 34** – Joint tensile properties measured at 21°C.

Tensile properties	MarM247/Ni-Zr joint 1230°C for 12 hours + SHT + HIP	Haynes 230/Ni-Zr joint 1230°C for 12 hours + SHT + HIP	Haynes 230	In738	MarM247
Tensile strength	736 MPa (107 ksi)	737 MPa (107 ksi)	860 MPa (125 ksi)	821 MPa (119 ksi)	960 MPa (139 ksi)
Yield strength	622 MPa (90 ksi)	718 MPa (104 ksi)	395 MPa (57 ksi)	683 MPa (99 ksi)	800 MPa (116 ksi)
Elongation (%)	3.7	1.3	50	4.0	7.9

**Table 35** – Joint tensile properties measured at 95°C.

Tensile properties	MarM247/Ni-Zr joint 1230°C for 12 hours + SHT + HIP	Haynes 230/Ni-Zr joint 1230°C for 12 hours + SHT + HIP	Haynes 230	In738	MarM247
Tensile strength	Not tested	739 MPa (107 ksi)	835 MPa (121 ksi)	883 MPa (128 ksi)	1014 MPa (147 ksi)
Yield strength	Not tested	726 MPa (105 ksi)	359 MPa (52 ksi)	752 MPa (109 ksi)	801 MPa (116 ksi)
Elongation (%)	Not tested	2.4	51	5.0	7.8

**Table 36** – Joint tensile properties measured at 315°C.

Tensile properties	MarM247/Ni-Zr joint 1230°C for 12 hours + SHT + HIP	Haynes 230/Ni-Zr joint 1230°C for 12 hours + SHT + HIP	Haynes 230	In738	MarM247
Tensile strength	Not tested	533 MPa (77 ksi)	787 MPa (114 ksi)	856 MPa (124 ksi)	1001 MPa (145 ksi)
Yield strength	Not tested	520 MPa (75 ksi)	324 MPa (47 ksi)	725 MPa (105 ksi)	807 MPa (117 ksi)
Elongation (%)	Not tested	2.0	52	5.0	7.7

**Table 37** – Joint tensile properties measured at 540°C.

Tensile properties	MarM247/Ni-Zr joint 1230°C for 12 hours + SHT + HIP	Haynes 230/Ni-Zr joint 1230°C for 12 hours + SHT + HIP	Haynes 230	In738	MarM247
Tensile strength	999 MPa (145 ksi)	638 MPa (92 ksi)	705 MPa (103 ksi)	876 MPa (127 ksi)	1014 MPa (147 ksi)
Yield strength	707 MPa (103 ksi)	624 MPa (90 ksi)	275 MPa (40 ksi)	745 MPa (108 ksi)	807 MPa (117 ksi)
Elongation (%)	3.7	1.9	53	5.1	7.8

**Table 38** – Joint tensile properties measured at 650°C.

Tensile properties	MarM247/Ni-Zr joint 1230°C for 12 hours + SHT + HIP	Haynes 230/Ni-Zr joint 1230°C for 12 hours + SHT + HIP	Haynes 230	In738	MarM247
Tensile strength	Not tested	511 MPa (74 ksi)	675 MPa (98 ksi)	828 MPa (120 ksi)	1021 MPa (148 ksi)
Yield strength	Not tested	497 MPa (72 ksi)	275 MPa (40 ksi)	690 MPa (100 ksi)	814 MPa (118 ksi)
Elongation (%)	Not tested	1.8	55	5.5	7.2

**Table 39** – Joint tensile properties measured at 870°C.

Tensile properties	MarM247/Ni-Zr joint 1230°C for 12 hours + SHT + HIP	Haynes 230/Ni-Zr joint 1230°C for 12 hours + SHT + HIP	Haynes 230	In738	MarM247
Tensile strength	743 MPa (108 ksi)	555 MPa (80 ksi)	435 MPa (63 ksi)	690 MPa (100 ksi)	790 MPa (115 ksi)
Yield strength	650 MPa (94 ksi)	541 MPa (78 ksi)	255 MPa (37 ksi)	137 MPa (76 ksi)	650 MPa (94 ksi)
Elongation (%)	3.4	1.5	65	7.5	5.0

**Table 40** – Joint tensile properties measured at 980°C.

Tensile properties	MarM247/Ni-Zr joint 1230°C for 12 hours + SHT + HIP	Haynes 230/Ni-Zr joint 1230°C for 12 hours + SHT + HIP	Haynes 230	In738	MarM247
Tensile strength	311 MPa (45 ksi)	267 MPa (39 ksi)	240 MPa (35 ksi)	414 MPa (60 ksi)	506 MPa (73 ksi)
Yield strength	240 MPa (35 ksi)	189 MPa (27 ksi)	145 MPa (21 ksi)	283 MPa (41 ksi)	312 MPa (45 ksi)
Elongation (%)	4.8	1.8	83	8.0	4.7

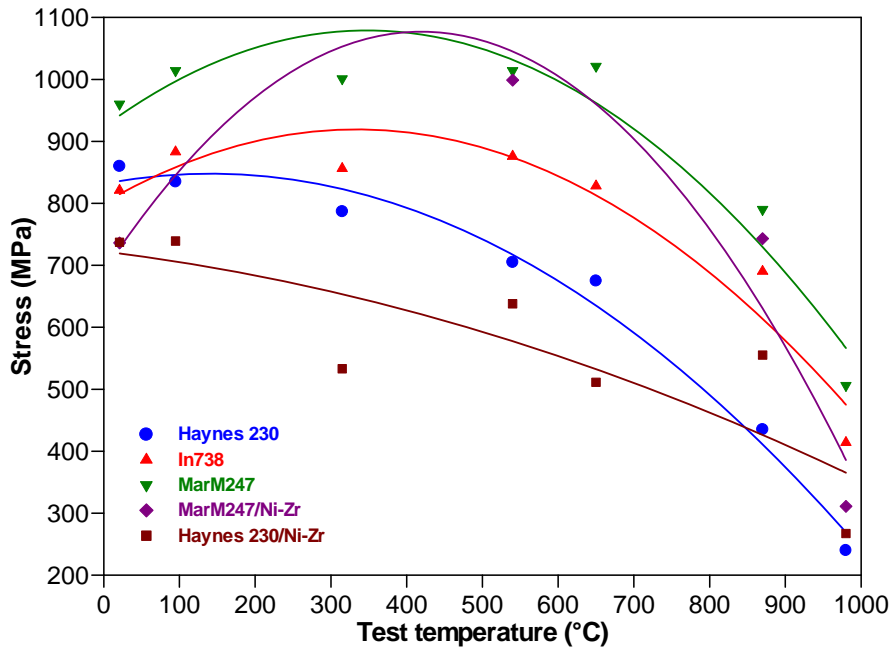


**Figure 136** – Tensile strength of Haynes 230, In738, MarM247, the MarM247/Ni-Zr braze joint and the Haynes 230/Ni-Zr braze joint as a function of test temperature.

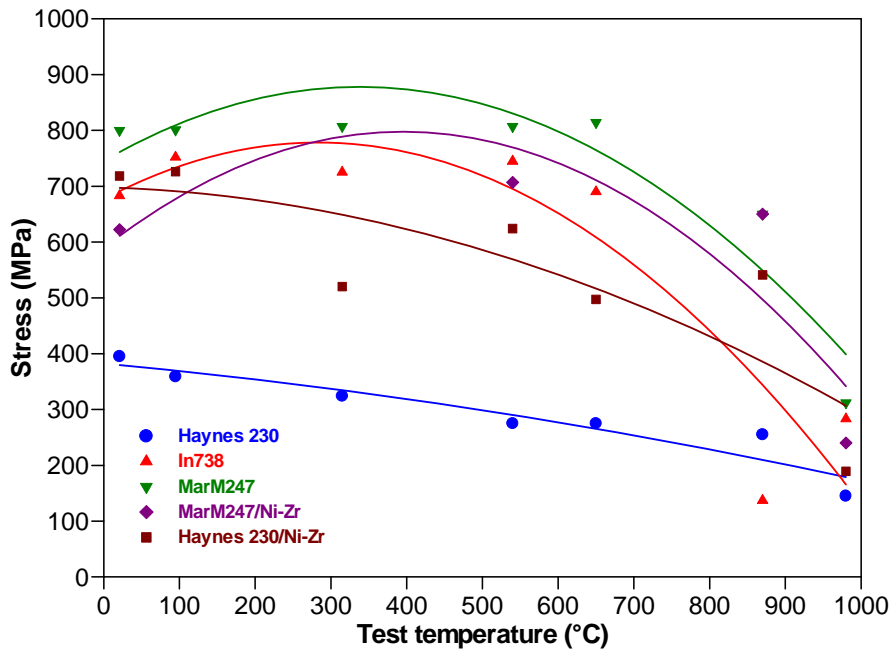


**Figure 137** – Yield stress of Haynes 230, In738, MarM247, the MarM247/Ni-Zr braze joint and the Haynes 230/Ni-Zr braze joint as a function of test temperature.

As shown **Table 34** and **Figures 136 and 137**, the room temperature tensile and yield strengths of the Haynes 230/Ni-Zr joint compared well with those of the MarM247/Ni-Zr joint. The high strength of the Haynes 230/Ni-Zr joint relative to that of the MarM247/Ni-Zr joint is attributed to it being in its highest strength condition (i.e. solution heat treated), whereas the MarM247/Ni-Zr joint was in the solution heat treated and partially aged condition. The MarM247/Ni-Zr joint only achieves its highest mechanical strength after secondary aging at 870°C.

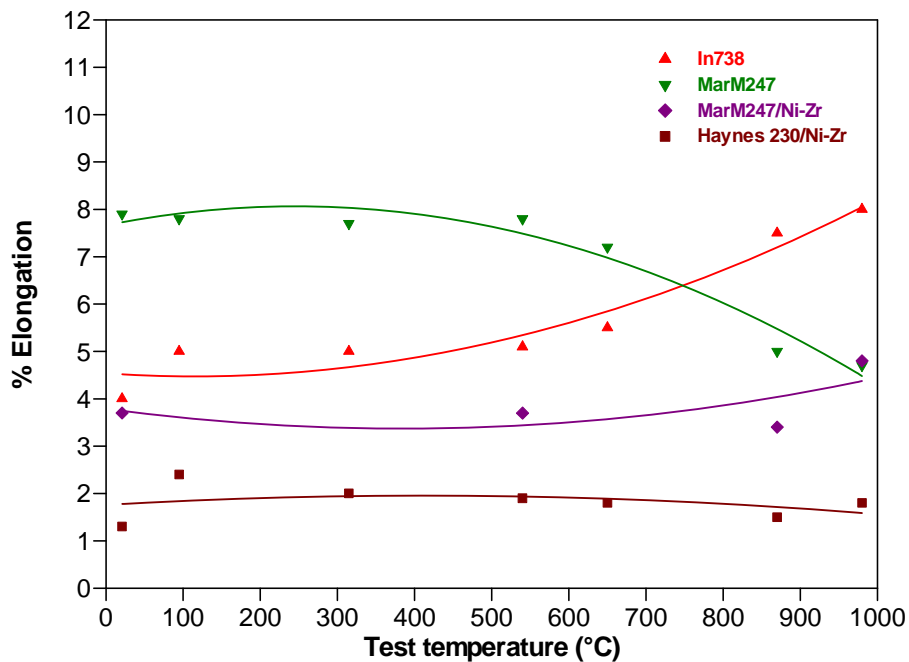


**Figure 138** – Percentage elongation of In738, MarM247, the MarM247/Ni-Zr braze joint and the Haynes 230/Ni-Zr braze joint as a function of test temperature.

As shown in **Table 34** and **Figure 138**, the room temperature ductility (expressed as percentage elongation) of the Haynes 230/Ni-Zr joint was surprisingly low, given that Haynes 230 material normally exhibits up to 50% elongation at room temperature. In contrast, the percentage elongation of the MarM247/Ni-Zr joint after solution heat treatment and HIP'ing (representing partial aging) achieved approximately 63% of the ductility of MarM247 and 75% of the measured ductility of the In738 base metal. Although not examined in more detail, it is postulated that the low ductility of the Haynes 230/Ni-Zr joint may be due to the braze alloy disrupting the continuity of the matrix, limiting the ductility of the joint. It is also possible that the majority of the plastic deformation in the joint was concentrated in the more ductile Haynes 230 powder particles, resulting in rapid work hardening of the austenitic matrix and premature failure during testing.

With an increase in the test temperature, the tensile and yield strengths of the MarM247/Ni-Zr joint increased, reaching peak strength values at a test temperature of approximately 540°C. At peak strength, the tensile and yield strength values of the MarM247/Ni-Zr joint attained 98% and 88%, respectively, of the tensile and yield strengths of MarM247 at the same temperature, and exceeded those of the In738 base metal. With a further increase in test temperature above 540°C, the tensile and yield strengths of the MarM247/Ni-Zr joint gradually decreased, following the same general trend as that observed for the MarM247 and In738 samples. The tensile and yield strengths of the Haynes 230/Ni-Zr joint gradually decreased with an increase in test temperature, following the same general trend as that of the Haynes 230 samples.

As shown in **Figure 138**, the ductility values (expressed as percentage elongation) of both joints were well below the ductility of the MarM247 and In738 samples at all test temperatures. The ductility of the MarM247/Ni-Zr joint increased slightly with an increase in test temperature, probably associated with the observed decrease in strength at higher temperatures. The measured ductility of the Haynes 230/Ni-Zr joint remained very low and did not vary to any significant extent with an increase in test temperature. It is postulated that



most of the plastic deformation during tensile testing was concentrated in the more ductile Haynes 230 powder particles, resulting in rapid work hardening and premature failure.

### 9.3.2 Creep rupture test results:

Creep rupture test results measured at various temperatures and stress levels are shown in **Table 41** and presented graphically in **Figure 139** in the form of a Larson-Miller plot. Also included are the creep rupture properties of In738 base metal and MarM247/Ni-Zr joints (from Chapter 7). Each value shown represents the average of three tests.

**Table 41** – Creep rupture properties of In738, Haynes 230 and the MarM247/Ni-Zr and Haynes 230/Ni-Zr joints (1.5 mm joint gap).

Test condition	Property	MarM247/Ni-Zr braze SHT + HIP	Haynes 230/Ni-Zr braze SHT + HIP	In738	Haynes 230
385 MPa at 650°C	Creep rupture life	Not tested	110 hours	Not tested	100 hours
	% Elongation		1.7		
	% Reduction in area		0.7		
185 MPa at 760°C	Creep rupture life	Not tested	212.8 hours	Not tested	100 hours
	% Elongation		0.3		
	% Reduction in area		1.7		
345 MPa at 845°C	Creep rupture life	24.4 hours	Not tested	27.4 hours	Not tested
	% Elongation	3.9		5.5	
	% Reduction in area	4.7		7.3	
95 MPa at 870°C	Creep rupture life	Not tested	114.6 hours	Not tested	100 hours
	% Elongation		0.6		
	% Reduction in area		0.9		
242 MPa at 900°C	Creep rupture life	22.1 hours	Not tested	29.8 hours	Not tested
	% Elongation	4.2		5.7	
	% Reduction in area	6.7		7.9	
41 MPa at 980°C	Creep rupture life	Not tested	252.2 hours	Not tested	100 hours
	% Elongation		1.7		
	% Reduction in area		11.1		
138 MPa at 980°C	Creep rupture life	17.7 hours	Not tested	21.2 hours	Not tested
	% Elongation	8.0		8.1	
	% Reduction in area	23.5		11.8	
24 MPa at 1040°C	Creep rupture life	Not tested	139.3 hours	Not tested	100 hours
	% Elongation		4.1		
	% Reduction in area		6.0		
14 MPa at 1095°C	Creep rupture life	Not tested	126.4 hours	Not tested	100 hours
	% Elongation		1.8		
	% Reduction in area		18.5		

SHT: Solution heat treatment at 1230°C for 4 hours.

HIP: Hot isostatic pressing at 1080°C for 4 hours.

It is evident from **Table 41** and **Figure 139** that the creep rupture properties of the Haynes 230/Ni-Zr joint were equivalent to that of Haynes 230 parent material, but inferior to those of the MarM247/Ni-Zr joint, and well below the creep rupture properties of the In738 base metal. The measured creep rupture life of the MarM247/Ni-Zr joint varied between 74% and 89% of that of the In738 base metal. It must be emphasized that the creep rupture properties of the MarM247/Ni-Zr joints are expected to improve on application of the full aging cycle (the results given in **Table 41** and **Figure 139** are relevant to the partially aged condition).

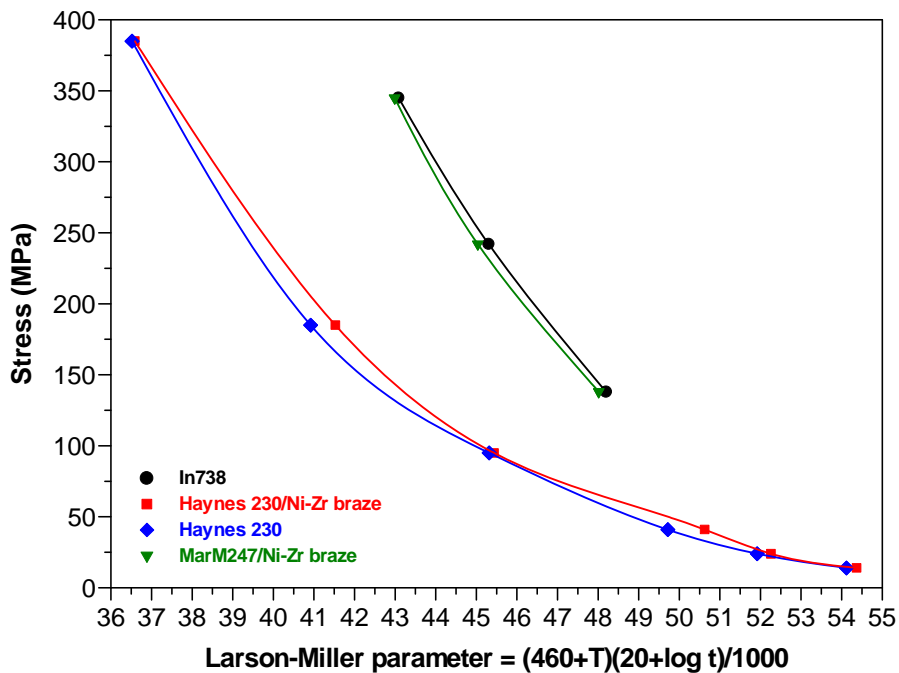


**Figure 139** – Creep rupture properties of In738, Haynes 230, the MarM247/Ni-Zr braze joint and the Haynes 230/Ni-Zr braze joint.

The creep rupture test results shown in **Table 41** confirm the observation (described in §9.3.1) of poor ductility in the case of the Haynes 230/Ni-Zr joints. Both the percentage elongation and the percentage reduction in area values were very low, especially in the high stress/low temperature creep regime. At higher test temperatures (such as 1040°C and 1095°), where the applied stress levels were lower, the ductility improved considerably. The MarM247/Ni-Zr joints displayed very good ductility, achieving up to 88% of the percentage elongation and reduction in area of the base metal (at a temperature of 980°C and an applied stress level of 138 MPa). Although equivalent base metal ductility was not obtained, the MarM247/Ni-Zr joints outperformed the commercially available B-containing brazes, for which elongation and reduction in area values below 30% are usually obtained in 1.5 mm wide joints. This suggests that the Ni<sub>5</sub>Zr intermetallic phase within the Ni-Zr joints does not embrittle the braze joints to the same extent as the boride phases commonly observed when B-containing braze alloys are used to fill in wide gaps.

#### 9.4) Conclusions

- Although the solid solution strengthened Haynes 230 Ni-base superalloy displays excellent ductility over a temperature range from room temperature to 980°C (well in excess of that documented for cast,  $\gamma'$ -strengthened alloys), Haynes 230/Ni-Zr braze joints displayed very poor ductility during testing. This may be due to the property mismatch between the Haynes 230 powder particles within the joint and the In738 parent material. During tensile testing, most of the plastic deformation is expected to take place in the more ductile Haynes 230 material, resulting in rapid work hardening of the austenitic matrix, and premature failure.
- The room temperature tensile and yield strengths of the Haynes 230/Ni-Zr joint compared well with those of the MarM247/Ni-Zr joint. With an increase in test

temperature, the tensile and yield strengths of the MarM247/Ni-Zr joint increased, reaching peak strength values at a test temperature of approximately 540°C. At peak strength, the tensile and yield strength values of the MarM247/Ni-Zr joint attained 98% and 88%, respectively, of the tensile and yield strengths of MarM247 at the same temperature, and exceeded those of the In738 base metal. With a further increase in test temperature above 540°C, the tensile and yield strengths of the MarM247/Ni-Zr joint gradually decreased, following the same general trend as that observed for the MarM247 and In738 samples. The tensile and yield strengths of the Haynes 230/Ni-Zr joint gradually decreased with an increase in test temperature, following the same trend as Haynes 230.

- The MarM247/Ni-Zr joints displayed excellent creep rupture properties, achieving between 74% and 89% of the creep rupture life of the In738 parent material. The creep rupture properties of the MarM247/Ni-Zr joints are expected to improve further on application of the full aging cycle. The MarM247/Ni-Zr joints also displayed very good ductility, achieving up to 88% of the ductility of the base metal. Although equivalent base metal ductility was not obtained, the MarM247/Ni-Zr joints outperformed the commercially available B-containing brazes.
- The Haynes 230/Ni-Zr joints displayed creep rupture properties equivalent to those of the Haynes 230 base metal, but inferior to those of the In738 parent material and the MarM247/Ni-Zr braze joints. Since the creep rupture properties of solid solution strengthened alloys, such as Haynes 230, are inferior to those of  $\gamma'$ -strengthened alloys, the poor creep rupture properties of the Haynes 230/Ni-Zr joints were not unexpected. The ductility values of the Haynes 230/Ni-Zr joint were, however, disappointingly low, especially in the high stress/low temperature creep regime. These low ductility values are attributed to the property mismatch between the braze joints and the parent material.
- Since the use of a more ductile matrix alloy in the braze joint did not result in any significant improvement in mechanical properties, the next chapter describes preliminary experiments aimed at improving the performance of the braze joints through the addition of chromium and boron to hypo-eutectic Ni-Hf braze alloys.

## **CHAPTER 10 - EXPERIMENT 8**

### **CHARACTERIZATION OF THE MICROSTRUCTURE AND PROPERTIES OF HYPO-EUTECTIC Ni-Cr-Hf AND Ni-Cr-Hf-B ALLOYS**

#### **10.1) Introduction**

The experiments described in earlier chapters focused on simple binary eutectic Ni-Zr or Ni-Hf braze alloys. Since the joint ductility could not be improved by using a more ductile solid solution strengthened matrix alloy within the joint (as described in Chapter 9), an attempt was made to improve the performance of the novel braze filler metals by producing a series of ternary and quaternary hypo-eutectic Ni-Hf alloys containing chromium and boron.

The aim of this experiment was therefore to develop ternary and quaternary hypo-eutectic braze alloys containing chromium and boron, and to characterize the microstructures of these alloys using microprobe analysis techniques.

#### **10.2) Experimental procedure**

Four off-eutectic experimental alloys were produced by melting various metal powders in a crucible at a temperature of 1500°C. The alloy compositions (in wt.%) are given below:

- Ni-13Cr-15Hf
- Ni-13Cr-20Hf
- Ni-13Cr-25Hf
- Ni-13Cr-25Hf-1B

After cooling, the alloy samples were mounted in resin and prepared using conventional metallographic techniques before being subjected to microstructural analysis using microprobe techniques. The mounted samples were carbon coated using a sputtering technique and electrically grounded with copper tape in order to minimize charging of the specimens by the microprobe electron beam. Calibration was performed using polished pure element standards.

Analysis conditions were established for either a 15 or 20 keV focused electron beam, adjusted to provide 35 nA of specimen current on pure nickel. Desired locations for analysis were selected by generating a backscattered electron (BSE) image before placing the instrument in "spot mode", during which the focused beam was directed to locations within the area shown in the BSE image. The EDS (energy dispersive x-ray spectroscopy) peak identifications were verified using a wavelength dispersive x-ray spectrometer (WDS), tuned to the elements of interest. X-ray intensity data were collected in triplicate at each phase location of interest. Measured x-ray counts were then converted to elemental weight percentages using commercially available algorithms.

A preliminary characterization of the mechanical properties of the alloys was performed by measuring the hardness of each specimen using a micro-Vickers hardness tester.

### 10.3) Results and discussion

#### 10.3.1 Ternary Ni-Cr-Hf alloys:

The microstructure of the Ni-13Cr-15Hf alloy after cooling is shown in **Figure 140**. The coarse dendritic phase (dark gray areas) was shown to have a composition of Ni-19.2Cr-1.6Hf (wt.%), identifying it as the Ni-rich  $\gamma$  phase. The white areas consisted of 53.7Ni-1.2Cr-45.1Hf (wt.%) and are most likely islands of  $\text{Ni}_7\text{Hf}_2$  intermetallic compound within the eutectic component. The fine eutectic component had a composition of Ni-9.0Cr-25.8Hf. This microstructure suggests that the alloy was hypo-eutectic, forming a primary Ni-rich  $\gamma$  phase on solidification. On reaching the eutectic temperature, the remaining liquid transformed to the eutectic mixture of  $\gamma$  and the  $\text{Ni}_7\text{Hf}_2$  intermetallic compound. The majority of the chromium present in this ternary alloy apparently partitioned to the  $\gamma$  phase on solidification.

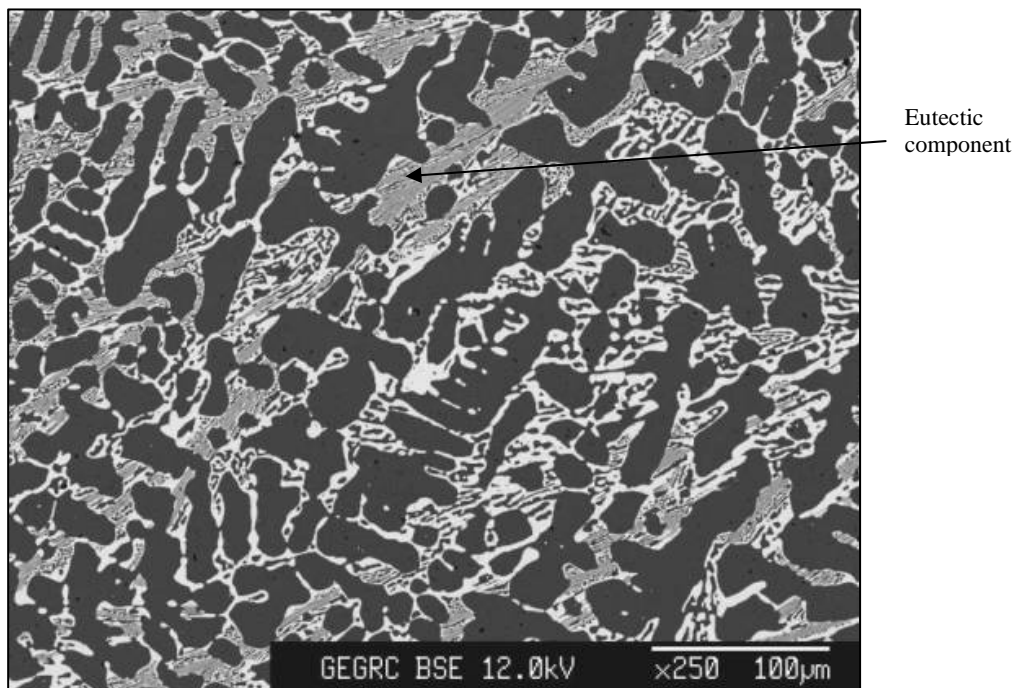


**Figure 140** - BSE image of the Ni-13Cr-15 Hf alloy showing primary  $\gamma$  dendrites, and a fine eutectic component consisting of  $\gamma$  phase and the  $\text{Ni}_7\text{Hf}_2$  intermetallic compound.

The microstructure of the Ni-13Cr-20Hf alloy, shown in **Figure 141**, is very similar to that of the alloy containing 15% Hf. The dark-etching phase was identified as Ni-rich  $\gamma$  dendrites (consisting of Ni-22.4Cr-1.4Hf), the white phase appeared to be the  $\text{Ni}_7\text{Hf}_2$  intermetallic compound (consisting of 53.8Ni-1.3Cr-44.9Hf), whereas the eutectic component had a composition of Ni-10.5Cr-25.2Hf (all compositions given as wt.%). This alloy also appeared to be hypo-eutectic, although at 20% Hf it is located closer to the eutectic point, resulting in less primary  $\gamma$  phase.

**Figure 142** shows the microstructure of the Ni-13Cr-25Hf alloy. The white areas were identified as  $\text{Ni}_7\text{Hf}_2$  intermetallic compound, with a nominal composition of 53.5Ni-0.8Cr-45.7Hf. The fine eutectic component consisted of  $\text{Ni}_7\text{Hf}_2$  intermetallic compound and the Ni-rich  $\gamma$  phase (dark gray regions). The eutectic component had a nominal composition of Ni-

15.1Cr-21.8Hf (all compositions given as wt.%). This microstructure suggests that the alloy was hypereutectic, forming a primary  $\text{Ni}_7\text{Hf}_2$  intermetallic phase on solidification. On reaching the eutectic temperature, the remaining liquid transformed to the eutectic mixture of Ni-rich  $\gamma$  phase and  $\text{Ni}_7\text{Hf}_2$  intermetallic compound. The majority of the chromium present in the alloy apparently partitioned to the  $\gamma$  phase on solidification.

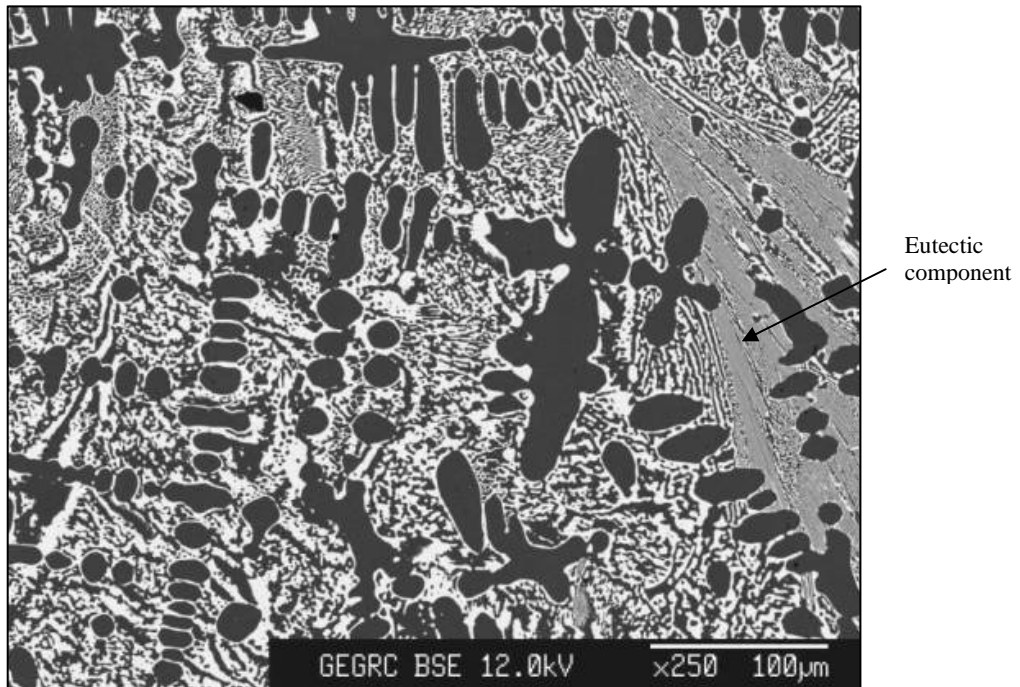


**Figure 141** - BSE image of the Ni-13Cr-20 Hf alloy showing primary  $\gamma$  dendrites, and a fine eutectic component consisting of  $\gamma$  phase and the  $\text{Ni}_7\text{Hf}_2$  intermetallic compound.



**Figure 142** - BSE image of the Ni-13Cr-25 Hf alloy showing primary  $\text{Ni}_7\text{Hf}_2$ , and a fine eutectic component consisting of  $\gamma$  phase and the  $\text{Ni}_7\text{Hf}_2$  intermetallic compound.

**Table 42** summarizes the measured chemical compositions of the eutectic components formed in each alloy on solidification. The binary Ni-Hf phase diagram shown in **Figure 49** indicates that the eutectic point in the binary Ni-Hf system is located at 30.5 wt.% Hf and a temperature of 1190°C. The addition of chromium therefore appears to shift the eutectic composition to lower Hf contents. The measured solidus and liquidus temperatures of the three ternary alloys are shown in **Table 43**. An increase in Hf content decreased the liquidus and increased in the solidus temperatures of the alloys. As expected, the solidus and liquidus temperatures of the ternary alloys were well above the Ni-Hf eutectic temperature of 1190°C.

**Table 42** – Chemical composition (wt.%) of the eutectic component observed in the ternary Ni-Cr-Hf alloys.

Alloy	Eutectic formed	Ni	Cr	Hf
Ni-13Cr-15Hf	Ni-rich $\gamma$ + Ni <sub>7</sub> Hf <sub>2</sub>	65.2	9.0	25.8
Ni-13Cr-20Hf	Ni-rich $\gamma$ + Ni <sub>7</sub> Hf <sub>2</sub>	64.3	10.5	25.2
Ni-13Cr-25Hf	Ni-rich $\gamma$ + Ni <sub>7</sub> Hf <sub>2</sub>	63.1	15.1	21.8

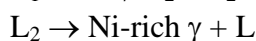
**Table 43** – Measured liquidus and solidus temperatures of the ternary Ni-Cr-Hf alloys.

Alloy	Solidus temperature	Liquidus temperature
Ni-13Cr-15Hf	1205°C	1337°C
Ni-13Cr-20Hf	1220°C	1304°C
Ni-13Cr-25Hf	1231°C	1291°C

### 10.3.2 Quaternary Ni-Cr-Hf-B alloy:

The microstructure of the quaternary Ni-13Cr-25Hf-1B alloy is shown in **Figure 143**. The addition of 1% B to the alloy resulted in the formation of a significant volume fraction of brittle borides (black phase). These boride particles were identified as chromium borides, with a composition of Ni-88.3Cr-0.0Hf-13.6B. The white areas were identified as the Ni<sub>7</sub>Hf<sub>2</sub> intermetallic phase (with a composition of Ni-0.7Cr-46.1Hf-0.3B), and the dark gray areas were shown to be the Ni-rich  $\gamma$  phase (containing Ni-25.9Cr-1.2Hf-0.2B). Analysis of the eutectic regions yielded compositions of Ni-11.0Cr-20.3Hf-2.0B (coarser eutectic component) and Ni-10.7Cr-16.9Hf-2.7B (fine eutectic regions). (All compositions given in wt.%).

The sequence of phase transformations on solidification of this alloy was probably:



### 10.3.3 Microhardness measurements:

In order to characterize the hardness of the phases within the braze alloys, Vickers microhardness tests were performed. The measured hardness values are given in **Table 44**. These results indicate that the chromium boride phase was significantly harder than the Hf-bearing intermetallic phase. This is consistent with the high ductility values obtained during earlier testing of Ni-Hf joints, compared with those typically found in B-containing brazes.

The high hardness of the eutectic component observed in the B-containing alloy suggests that the chromium boride phase participated in the eutectic reaction, possibly resulting in the formation of a ternary Cr boride/ $\gamma$ / $\text{Ni}_7\text{Hf}_2$  eutectic component.

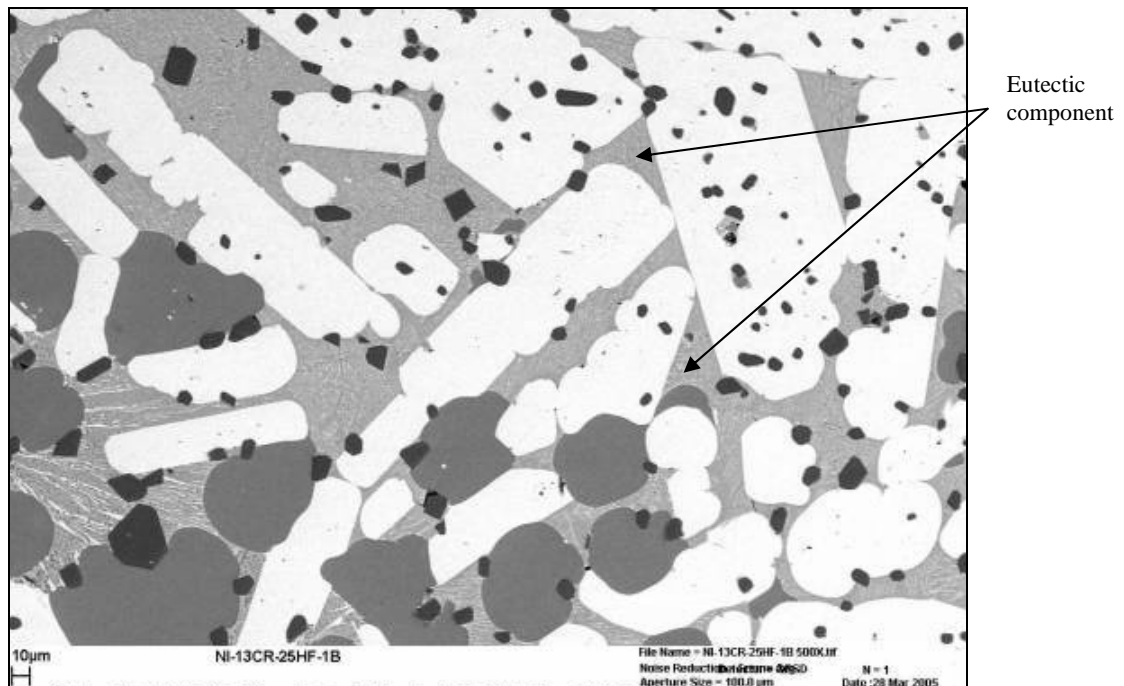


**Figure 143** - BSE image of the Ni-13Cr-25 Hf-1B alloy showing the  $\text{Ni}_7\text{Hf}_2$  phase (white), Ni-rich  $\gamma$  (dark gray), chromium borides (black) and a possible ternary eutectic component consisting of  $\gamma$  phase, Cr boride, and the  $\text{Ni}_7\text{Hf}_2$  intermetallic compound.

**Table 44** – Measured microhardness values of various phases observed in the ternary and quaternary alloys.

Alloy	Microhardness, $H_v$							
	$\gamma$ phase		Eutectic constituent		Boride phase		Other	
	Average	Standard deviation	Average	Standard deviation	Average	Standard deviation	Average	Standard deviation
Ni-13Cr-15Hf	242	19	294	56	N/A	N/A	N/A	N/A
Ni-13Cr-20Hf	309	19	322	72	N/A	N/A	N/A	N/A
Ni-13Cr-25Hf	398	32	324	30	N/A	N/A	N/A	N/A
Ni-13Cr-25Hf-1B	326	93	746	108	1150	240	350	43

**Table 45** summarizes the microprobe results, and displays the chemical compositions of the microstructural constituents observed within the ternary and quaternary alloys.

#### 10.4) Conclusions

- The ternary Ni-13Cr-15Hf and Ni-13Cr-20Hf alloys appeared to be hypo-eutectic, and consisted of primary Ni-rich  $\gamma$  dendrites (with approximately 20% Cr in solution), and a eutectic component consisting of  $\gamma$  phase and  $\text{Ni}_7\text{Hf}_2$  intermetallic compound. Increasing the Hf content from 15% to 20% reduced the amount of primary  $\gamma$  phase. The Ni-13Cr-25Hf alloy appeared to be hypereutectic, with a primary  $\text{Ni}_7\text{Hf}_2$  phase and a eutectic



component consisting of  $\gamma$  and  $\text{Ni}_7\text{Hf}_2$ . Since the eutectic point in binary Ni-Hf alloys is located at approximately 30.5% Hf, the addition of chromium apparently shifted the eutectic composition to lower Hf contents.

**Table 45** – The chemical compositions of various phases within the ternary and quaternary alloys (all compositions given as wt.%).

Alloy	Microstructural constituent	Transformation	Weight %			
			Ni	Cr	Hf	B
Ni-13Cr-15Hf	Ni-rich $\gamma$	Primary	79	19.2	1.6	-
	$\text{Ni}_7\text{Hf}_2$	Eutectic	55.5	1.2	45.1	-
	Eutectic component $\left\{ \begin{array}{l} \text{Ni}_7\text{Hf}_2 \\ \gamma \end{array} \right.$	Eutectic	65.2	9	25.8	-
Ni-13Cr-20Hf	Ni-rich $\gamma$	Primary	75.9	22.4	1.4	-
	$\text{Ni}_7\text{Hf}_2$	Eutectic	55.9	1.3	44.9	-
	Eutectic component $\left\{ \begin{array}{l} \text{Ni}_7\text{Hf}_2 \\ \gamma \end{array} \right.$	Eutectic	64.3	10.5	25.2	-
Ni-13Cr-25Hf	$\text{Ni}_7\text{Hf}_2$	Primary	54.9	0.8	45.7	-
	Eutectic component $\left\{ \begin{array}{l} \text{Ni}_7\text{Hf}_2 \\ \gamma \end{array} \right.$	Eutectic	63.1	15.1	21.8	-
Ni-13Cr-25Hf-1B	$\text{Ni}_7\text{Hf}_2$	Primary	54.9	0.7	46.1	0.3
	Ni-rich $\gamma$	Primary	73.2	25.9	1.2	0.2
	Cr boride	Primary	2.6	88.3	0.0	13.6
	Eutectic component $\left\{ \begin{array}{l} \text{Ni}_7\text{Hf}_2 \\ \gamma \\ \text{Cr boride} \end{array} \right.$	Eutectic	65.9	11.0	20.3	2.0
			70.2	10.7	16.9	2.7

- An increase in the Hf content of the experimental alloys lowered the liquidus temperature, but increased the solidus temperature. Since single-crystal Ni-base superalloys can be processed at temperatures up to 1310°C, only the Ni-13Cr-25Hf alloy holds any potential for production brazing. The liquidus temperatures of the Ni-13Cr-20Hf and Ni-13Cr-15Hf alloys exceeded 1300°C.
- The quaternary Ni-13Cr-25Hf-1B alloy consisted of a coarse  $\text{Ni}_7\text{Hf}_2$  phase, islands of Ni-rich  $\gamma$  (with Cr in solution), a ternary eutectic component ( $\text{Ni}_7\text{Hf}_2$ ,  $\gamma$  and Cr boride) and a significant volume fraction of chromium boride particles. The boride particles were shown to be considerably harder than the  $\text{Ni}_7\text{Hf}_2$  intermetallic phase. This difference in hardness may account for the high ductility and good LCF properties of the Ni-Hf braze joints, compared with those of braze alloys containing B as a melt point depressant.